Geophysical and geochemical nature of relaminated arc-derived lower crust underneath oceanic domain in southern Mongolia

Alexandra Guy, Karel Schulmann, V. Janoušek,, P. Štípská, R Armstrong,, E Belousova,, A Dolgopolova,, Reimar Seltmann, O Lexa,, Y Jiang,, et al.

AGU PUBLICATIONS

Tectonics

RESEARCH ARTICLE
10.1002/2015TC003845

Key Points:
- Gravity modelling suggests a homogeneous felsic lower crust
- Granite geochemistry shows a juvenile felsic gneiss/granulite lower crust
- Oceanic upper crust is underlain by allochtonous, arc-derived material

Correspondence to:
A. Guy,
alexandra.guy@gmail.com

Citation:
Guy, A., et al. (2015), Geophysical and geochemical nature of relaminated arc-derived lower crust underneath oceanic domain in southern Mongolia, *Tectonics*, *34*, 1030–1053, doi:10.1002/2015TC003845.

Received 5 FEB 2015
Accepted 21 APR 2015
Accepted article online 24 APR 2015
Published online 27 MAY 2015

Geophysical and geochemical nature of relaminated arc-derived lower crust underneath oceanic domain in southern Mongolia

Alexandra Guy[1], Karel Schulmann[1,2], Vojtěch Janoušek[1], Pavla Štípská[1,2], Robin Armstrong[3], Elena Belousova[4], Alla Dolgopolova[3], Reimar Seltmann[3], Ondrej Lexa[1,5], Yingde Jiang[1,5], and Pavel Hanžl[1]

[1]Centre for Lithospheric Research, Czech Geological Survey, Prague 1, Czech Republic, [2]Institut de Physique du Globe, EOST CNRS UMR7516, Université de Strasbourg, France, [3]Centre for Russian and Central EurAsian Mineral Studies, Department of Earth Sciences, Natural History Museum, London, UK, [4]ARC Centre of Excellence for Core to Crust Fluid Systems (CCFS) and GEMOC, Macquarie University, Sydney, New South Wales, Australia, [5]Institute of Petrology and Structural Geology, Faculty of Science, Charles University, Prague 2, Czech Republic

Abstract The Central Asian Orogenic Belt (CAOB) in southern Mongolia consists of E-W trending Neoproterozoic cratons and Silurian-Devonian oceanic tectonic zones. Previous study revealed that the Early Paleozoic accretionary wedge and the oceanic tectonic zone are underlain by a layer giving a homogeneous gravity signal. Forward gravity modelling suggests that this layer is not formed of high-density material typical of lower oceanic crust but is composed of low- to intermediate-density rocks resembling continental crust. The nature of this lower crust is constrained by the whole-rock geochemistry and zircon Hf isotopic signature of abundant Late Carboniferous high-K calc-alkaline and Early Permian A-type granitoids intruding the two Early Paleozoic domains. It is possible to explain the genesis of these granitoids by anatexis of juvenile, metaigneous (tonalitic-gabbroic) rocks of Late Cambrian age, the source of which is presumed to lie in the "Khantaishir" arc (520–495 Ma) further north. In order to test this hypothesis, the likely modal composition and density of Khantaishir arc-like protoliths are thermodynamically modelled at granulite- and higher amphibolite-facies conditions. It is shown that the current average density of the lower crust inferred by gravity modelling (2730 ± 20 kg/m^3) matches best metamorphosed leucotonalite to diorite. Based on these results, it is now proposed that Mongolian CAOB has an architecture in which the accretionary wedge and oceanic upper crust is underlain by allochthonous lower crust that originated in a Cambrian arc. A tectonic model explaining relamination of allochthonous felsic to intermediate lower crust beneath mafic upper crust is proposed.

1. Introduction

Accretionary orogens are formed by two contrasting processes: net crustal growth resulting from magmatic activity above the subduction zone and continental construction resulting from lateral accretion of continental and oceanic crustal fragments, oceanic arcs, and accretionary wedges to continental nuclei [*Jahn*, 2004; *Cawood et al.*, 2009; *Safonova et al.*, 2011]. The relative contribution of the two processes to net continental growth is hard to decipher because of the difficulty of quantifying the different stages of evolution in ancient orogenic systems and the incompleteness of tectonic evolution in modern accretionary orogens.

Attempts have been made in previous studies to characterize and classify the vertical structure of continental crust using geophysical and geochemical properties in different geodynamic settings [e.g., *Rudnick and Fountain*, 1995; *Christensen and Mooney*, 1995; *Fliedner and Klemperer*, 2000; *Holbrook et al.*, 1999]. Based on average seismic velocities, the crust is conventionally divided into three layers (upper, middle, and lower). In general, the *P* wave velocity increases with depth, but this does not mean that the homogeneous physical behavior of each layer implies lithological homogeneity. *Rudnick and Fountain* [1995] and *Christensen and Mooney* [1995] distinguished six types of continental crust (shield, collisional orogen, back arc, magmatic arc, extended crust, and passive margin), each with a characteristic thickness. Taking into account the contrasting compositions of these different types of crust, the structure of accretionary orogens consisting of different terranes [*Windley et al.*, 2007] should also be distinctly heterogeneous, both horizontally and vertically. Because the accretionary orogens are commonly precursors of collisional

orogens [*Schulmann and Paterson*, 2011], the knowledge of their vertical structure and composition of the lower crust is crucial for understanding the mechanisms of continental growth.

The direct approach to understanding lower crustal composition is based on the study of deep crustal xenoliths, usually sampled by young volcanic rocks. The petrology and whole-rock geochemistry of such samples can be analyzed directly [e.g., *Rudnick*, 1992; *Downes*, 1993]. Alternatively, indirect information may be obtained from whole-rock geochemical studies of granitoids that can be used to constrain the chemistry of the lower crustal sources from which they were derived [e.g., *Clemens*, 2003; *Kemp and Hawkesworth,* 2003; *Brown,* 2007, 2013, and references therein]. These analyses are often supplemented by isotopic data, especially in situ Hf isotopic analysis of dated zircons, in order to determine the composition and mean crustal residence times of their source rocks [*Belousova et al.,* 2010; *Kemp and Hawkesworth,* 2014, and references therein].

The Central Asian Orogenic Belt (CAOB) or Altaids is one of the largest accretionary systems of the World covering one third of Asia [*Şengör et al.*, 1993]. It is composed of accreted Precambrian continental segments with a strong Neoproterozoic overprint [*Rojas-Agramonte et al.*, 2011], Neoproterozoic ophiolites and accretionary complexes [*Khain et al.*, 2003] and Siluro-Devonian oceanic crust [*Zonenshain et al.*, 1975; *Kröner et al.*, 2010; *Safonova et al.*, 2011], and Ordovician, Devonian, and Carboniferous arcs and back arcs [*Badarch et al.*, 2002; *Economos et al.*, 2008; *Demoux et al.*, 2009]. The existing geophysical data [*Mordvinova et al.*, 2007; *Mordvinova and Artemyev*, 2010; *Teng et al.*, 2013; *Zhang et al.*, 2014] show that the thickness of the crust in the southern part of the CAOB is near constant at ~45 km. Recently, *Guy et al.* [2014b] showed that the upper crust in this region is ~20 km thick and heterogeneous, whereas the underlying 25 km thick lower crust is geophysically uniform.

In the present paper, the architecture of the lower crust in the southern CAOB is assessed by gravity modelling, and its composition and possible tectonic affinity are constrained by the geochemistry of granitic rocks. Once the chemical and petrological compositions of the lower crustal source of granitic rocks are determined, its density can be thermodynamically modelled and compared to geophysical observations. This combined approach is used not only to characterize the nature of thick, uniform, and compositionally anomalous lower crust underlying the heterogeneous upper crustal material in Gobi-Altai and Trans-Altai zones of the Mongolian CAOB but also to underline the importance of relamination processes [*Hacker et al.*, 2011] in accretionary orogens.

2. Geological Setting and Geophysical Background

2.1. Lithotectonic Zonation of the South Mongolian CAOB

The CAOB was formed by accretion of magmatic arcs, back arc and fore arc, accretionary complexes, passive margins, and continental basement blocks [e.g., *Şengör et al.*, 1993]. The period of accretion is considered to have lasted from the Mesoproterozoic to the Early Carboniferous [*Badarch et al.*, 2002] and was followed by voluminous late- to post-tectonic granitoid intrusions of Late Carboniferous to Permian age [*Jahn*, 2004]. *Badarch et al.* [2002] divided the Mongolian CAOB into a large number of cratonic, metamorphic, passive-margin, island arc, back arc, and accretionary-wedge terranes. The detailed lithostratigraphic, geochronological, and structural study of *Kröner et al.* [2010] has shown that the terrane mosaic of the south Mongolian CAOB can be simplified into five lithotectonic zones bounded by strike-slip faults or sutures (Figure 1): (1) the Baydrag Continent, (2) the Lake Zone, (3) the Gobi-Altai Zone, (4) the Trans-Altai Zone, and (5) the South Gobi Zone.

The *Lake Zone* consists of a Neoproterozoic to Early Cambrian accretionary wedge [*Zonenshain and Kuzmin*, 1978; *Štípská et al.*, 2010] and is composed of volcanic arcs and accretionary prisms thrust over the Precambrian basement rocks of the Baydrag Continent lying to the north [*Didenko et al.,* 1994; *Kozakov et al.*, 1997, 2002a]. Recently, *Janoušek et al.* [2014] provided evidence for the existence of a large Late Cambrian "Khantaishir" magmatic arc rimming the southern border of the Lake Zone.

The *Gobi-Altai Zone* consists of thick Cambrian and Ordovician volcanosedimentary sequences recently interpreted as a giant accretionary wedge [*Xiao et al.*, 2010] covered by folded passive margin deposits of Silurian and Devonian age [*Zonenshain*, 1973; *Zorin et al.*, 1993] alternating with gneiss domes made of high-grade metamorphic rocks, migmatites, and granulites [*Kozakov et al.*, 2002b; *Kröner et al.*, 2010;

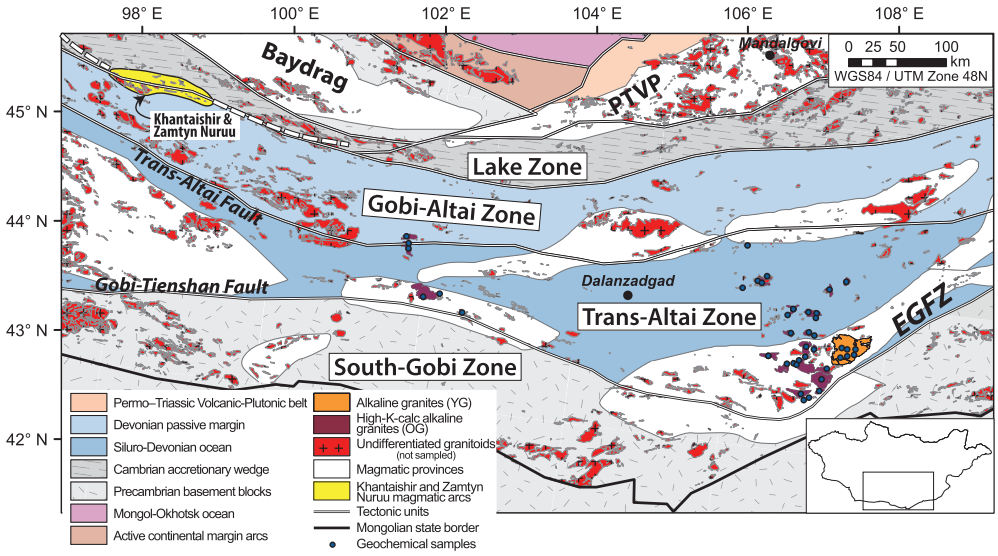

Figure 1. Tectonic map of southern Mongolia showing the distribution of the continental and oceanic domains. The magmatic provinces corresponding to magnetic anomalies [*Guy et al.*, 2014b] are accompanied by the accurate location of granitoids and superimposed on the tectonic units. The white dashed lines denote the possible extent of the Khantaishir and Zamtyn Nuruu magmatic arcs. PTVP: Permo-Triassic Volcanic Plutonic belt; EGFZ: East Gobi Fault Zone.

Lehmann et al., 2010]. The growth of migmatitic domes was constrained by dating of syntectonic granitoids at Late Devonian to Early Carboniferous [*Lehmann et al.*, 2010; *Broussolle et al.*, 2015].

The rocks of the *Trans-Altai Zone* consist of Devonian to Early Carboniferous volcanoclastic, mainly graywacke-dominated deposits associated with massive volcanic rocks representing Siluro-Devonian volcanic arcs and back arcs (Figure 2). *Ruzhentsev et al.* [1985] and *Ruzhentsev et al.* [1992] showed that the basement of the Siluro-Devonian volcanosedimentary sequences is always ultramafic, which indicates that the entire zone represented an oceanic floor in Early Paleozoic times. Recently, *Jian et al.* [2014] dated several gabbroic units in the Trans-Altai Zone at ~523–511 Ma and proposed that the opening of the Palaeo-Asian Ocean started in the Late Cambrian. It is therefore likely that passive margin sequences in the Gobi-Altai and exhumed mantle in the Trans-Altai Zone reflect progressive formation of Palaeo-Asian

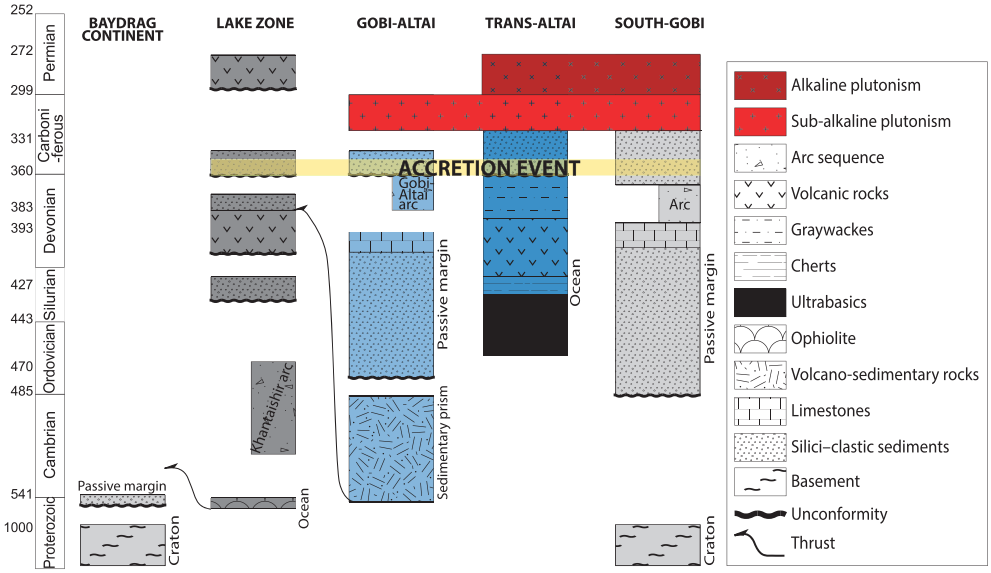

Figure 2. Simplified lithostratigraphic columns for individual tectonic zones located in southern Mongolia.

oceanic crust during the Late Cambrian to Early Devonian [*Zonenshain*, 1973; *Zorin et al.*, 1993; *Lamb and Badarch*, 2001]. The ophiolites were often thrust over volcanosedimentary sequences during Early Carboniferous convergence, and therefore, the general structure of the Trans-Altai Zone has been interpreted as an imbricated intraoceanic ophiolitic system [*Ruzhentsev*, 2001; *Guy et al.*, 2014a].

Finally, the Gobi-Tianshan Fault Zone separates the Trans-Altai Zone from the *South Gobi Zone* in the southernmost part of the CAOB. The South Gobi Zone consists of a Precambrian basement covered by Ordovician and Silurian siliciclastic sediments, Devonian volcanosedimentary rocks, and Carboniferous volcanic rocks (Figure 2). The Ordovician to Silurian rocks are typical continental-margin sediments [*Zonenshain*, 1973; *Johnson et al.*, 2008; *Lehmann et al.*, 2010], whereas Upper Devonian to Carboniferous strata consist of thick volcanic sequences topped by Permian continental sedimentary deposits.

All tectonic domains forming the Mongolian CAOB were affected by pronounced N-S Permo-Triassic shortening that resulted in the formation of subvertical E-W trending high-strain zones separated by weakly deformed domains [*Lehmann et al.*, 2010; *Leonov*, 2012; *Guy et al.*, 2014a]. The high-strain zones are characterized by upright folds, subvertical cleavage, and the steepening of lithological units [*Guy et al.*, 2014a]. The Trans-Altai and South Gobi zones are intruded by Late Carboniferous and Permian granitoids located in distinct linear zones, mostly parallel to the main tectonic boundaries [*Kovalenko et al.*, 2004; *Yarmolyuk et al.*, 2008].

2.2. Composition and Thickness of the South Mongolian Lower Crust—Xenolith Evidence

Unfortunately, studies of xenoliths constraining the deep crustal composition of the CAOB are rare and inconclusive. The information that exists comes mainly from a few xenoliths obtained from the Cenozoic volcanic massifs located in the Tariat depression north of the Hangay Dome and from the Dariganga volcanic field in eastern Mongolia. These intermediate to mafic xenoliths are orthopyroxene, clinopyroxene, and garnet-clinopyroxene granulites and spinel peridotites derived from near the crust-mantle boundary [*Stosch et al.*, 1995; *Kopylova et al.*, 1995; *Ionov*, 2002]. Lower crustal xenoliths in Cenozoic basalts from the Gobi-Altai and Trans-Altai zones are intermediate orthopyroxene- and clinopyroxene-bearing granulites and unusual felsic rocks [*Barry et al.*, 2003]. The pressure estimates of 14.5 ± 1.5 kbar correspond to a Cenozoic crustal thickness of 45–50 km [*Stosch et al.*, 1995]. However, in order to determine the present crustal thickness, geophysical data are needed.

3. Geophysical Characterization of the Lower Crust

Guy et al. [2014b] carried out a detailed analysis of the geophysical structures of the south Mongolian CAOB using gravity and airborne magnetic data. Their analysis showed that the boundaries of the tectonic zones are not systematically defined by strong gravity and magnetic gradients and that the geophysical heterogeneity of the upper crust is related to Permo-Triassic deformation and magmatism. The match-filtering method indicated that this structural heterogeneity disappears at a depth of ~20 km. Here, we investigate the geometry and density distribution of the deeper part of the south Mongolian crust. For this purpose, forward gravity modelling constrained by existing seismic data and geological data was carried out along selected profiles perpendicular to the general structure of the CAOB.

3.1. Gravity Pattern of Southern Mongolia

Gravity data used for this study are the DNSC08 free air gravity model [*Andersen and Knudsen*, 2009] available at a spatial resolution of 2×2 min, which contain satellite, airborne, and terrestrial measurements. In order to construct the complete Bouguer anomaly map presented in Figure 3, this data set has been corrected for the topography using the standard density of 2.67 g/cm^3 and a digital elevation model at a spatial resolution of 2×2 min based on the ETOPO2 global relief model [*Amante and Eakins*, 2009]. The Bouguer anomalies vary from −245 mGal to −125 mGal, and three principal NE–SW trending zones stand out: (1) a large-scale gravity low in the north-west, (2) a large-scale gravity high in the south-east, and (3) a transitional area between these two gravity zones marked by large-amplitude and short-wavelength anomalies oriented NNW-SSE.

In order to highlight the boundaries of the density units, isolines of the tilt of the complete Bouguer anomaly are superimposed on the map together with the WNW-ESE oriented interpretative lineaments [*Miller and Singh*, 1994; *Blakely*, 1996] (Figure 3). A relatively smooth and regular gradient is observed in the NNE contrasting with the sharp gradients present in western and southern areas. This indicates a change in

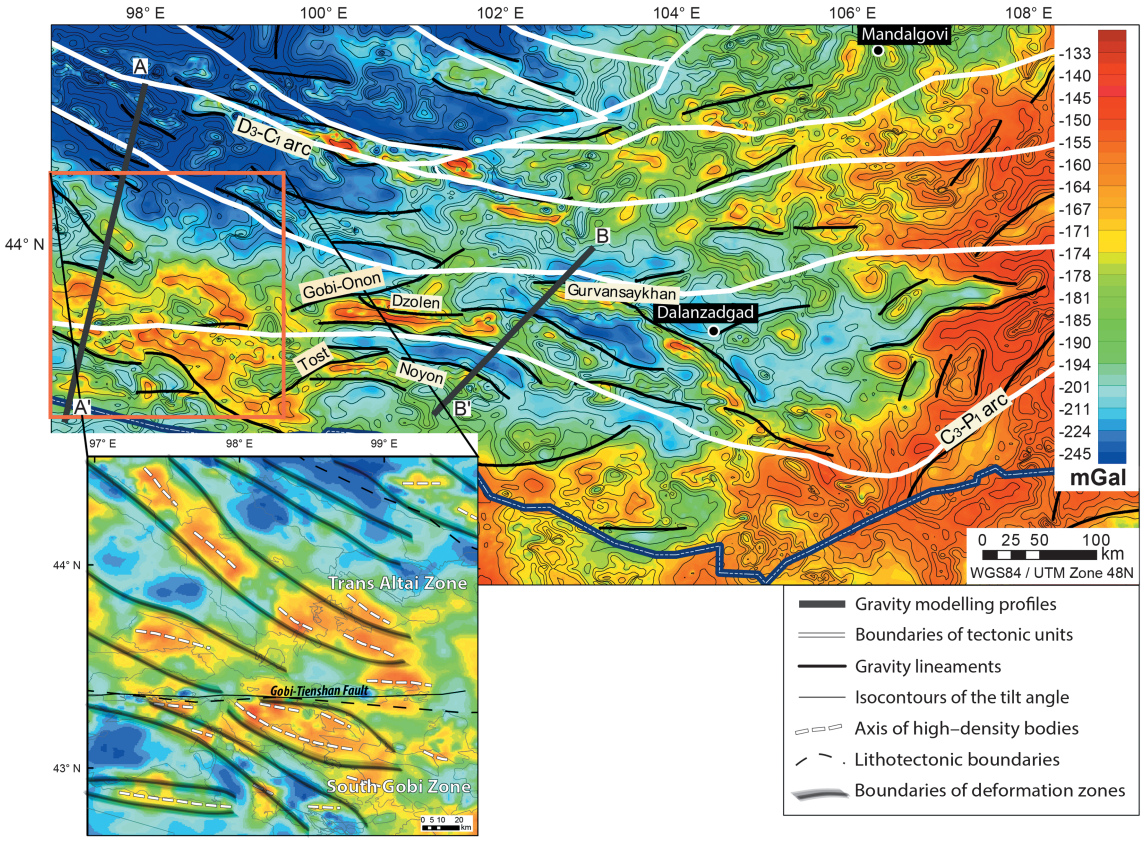

Figure 3. Complete Bouguer anomaly map of southern Mongolia with the isolines of the tilt and the lineaments (black lines) superimposed. The inset shows that the regional gravity fabrics are correlated with high-strain zones.

lithospheric structure that took place during the Cretaceous episode of extension [*Guy et al.*, 2014b] accompanied by the lithosphere delamination affecting the whole region of NE Asia [*Chen et al.*, 2008]. A pronounced gravity low in the north-west of the map correlates with the southern margin of the Permian Hangay Dome anomaly located further north [*Petit et al.*, 2002; *Yarmolyuk et al.*, 2013].

In the southern part of the map, elongated gravity highs are present which coincide spatially with mountain ranges. *Guy et al.* [2014b] showed that these anomalies correspond to zones of Permo-Triassic deformation (inset in Figure 3) reactivated during Cenozoic transpressive faulting [*Cunningham et al.*, 2009]. According to *Guy et al.* [2014b], localized steepening of ultramafic slivers and mafic volcanic rocks in these deformation zones are responsible for elongated high-amplitude anomalies.

3.2. Forward Modelling: Constraints and Implementation

The modelling of the Moho depth is constrained by existing seismic data. PASSCAL 1991–1992 [*Mordvinova and Artemyev*, 2010] and MOBAL 2003 [*Mordvinova et al.*, 2007] are two velocity models based on the inversion of the *P*-to-*S* wave receiver functions located in the central part of Mongolia (Figure 4a). Each about 1000 km long, the PASSCAL 1991–1992 section strikes NW-SE and the MOBAL 2003 strikes N-S. The sections both start in the southern part of the Siberian Craton, cross the Baikal Rift zone, and terminate before reaching the Gobi-Altai Zone. The velocity sections display a rather flat Moho topography dipping gently towards the south from 42 to 46 km underneath Mongolia, but the Moho depth underneath the Baikal Rift zone with an average depth of 35 km is obviously shallower (Figures 4b and 4c). This relatively flat shape of the Moho is confirmed by a combined topography, gravity, and traveltime residuals inversion [*Petit et al.*, 2008]. A deep seismic sounding study [*Teng et al.*, 2013] (Figure 4d) and a seismic reflection profile [*Zhang et al.*, 2014] across the Solonker suture in the north of China (Figure 4e) reveal a flat topography of the Moho at a depth of ~45 km. All these studies point to a Moho depth of about 45 km,

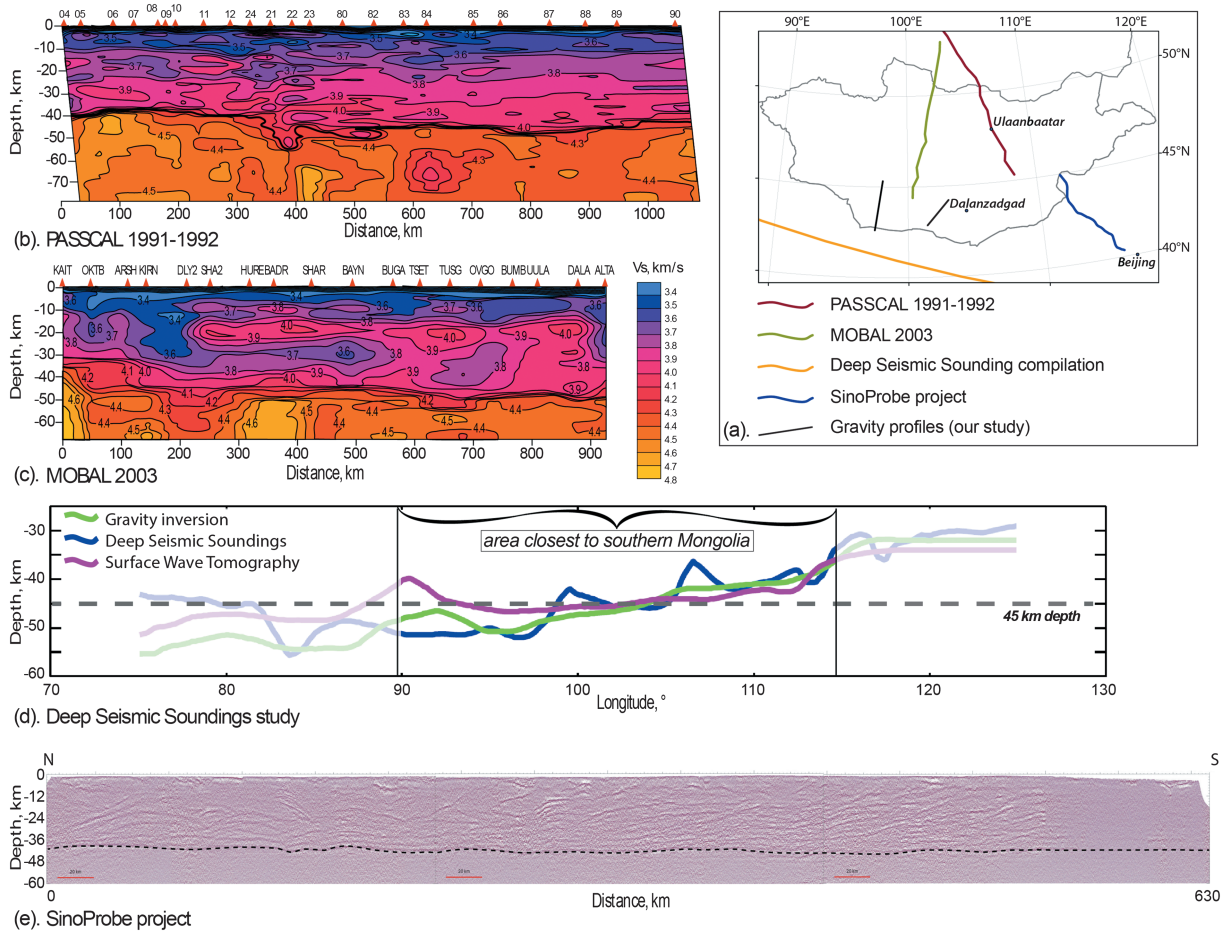

Figure 4. Comparison of the different seismic studies located within southern Mongolia. (a). Location of the four seismic sections. (b). 2-D *S* wave velocity section from PASSCAL 1991–1992 obtained by inversion of receiver functions [modified from *Mordvinova and Artemyev,* 2010]. The color scale is the same as for the MOBAL 2003 seismic section below. (c). 2-D *S* wave velocity section from MOBAL 2003 obtained by inversion of receiver functions [modified from *Mordvinova et al.,* 2007]. (d). Transect of the deep seismic sounding study compared with the results of gravity inversion and surface wave tomography studies [modified from *Teng et al.*, 2013]. (e). Seismic reflection section where approximate depth was estimated using an average velocity of 6 km/s [modified from *Zhang et al.*, 2014].

deepening to 50 km north of our study area, i.e., below the Hangay Dome. Therefore, based on the seismic studies described above, an average depth to the Moho of 45 km is used in our models.

In addition, the gravity modelling can be constrained by geological data such as lithostratigraphy, structural studies, and the petrophysical properties of rocks. The modelling has been carried out along two profiles parallel to geological cross sections of *Lehmann et al.* [2010] and *Guy et al.* [2014a] using the GM-SYS 2D modelling software. A surface geological map at 1:500,000 scale and geological interpretations of the potential field data [*Guy et al.,* 2014b] have been used to constrain the modelling. Because of the lack of direct density measurements in southern Mongolia, the densities attributed to the modelled bodies come from general rock density tables [e.g., *Telford et al.*, 1990].

Generally, magnetic data are used to constrain the geometry of the structures in the upper crust. However, in their absence, the initial strategy was to model intermediate- to short-wavelength gravity anomalies corresponding to isostatic residual Bouguer anomalies (Figure 5a). This provided constraints on the shape and the depth of the crustal density units. The crust of southern Mongolia was initially divided into distinct upper, middle, and lower layers for each tectonic zone based on the crustal model of *Rudnick and Fountain* [1995] and *Christensen and Mooney* [1995]. The mantle layer was assumed to be laterally homogeneous, with a density of 3200 kg/m^3. Following this modelling step, the complete Bouguer gravity anomalies containing the long wavelength of the signal were used to adjust the densities of the lower crustal structures maintaining realistic density contrasts between the different units (Figure 5b).

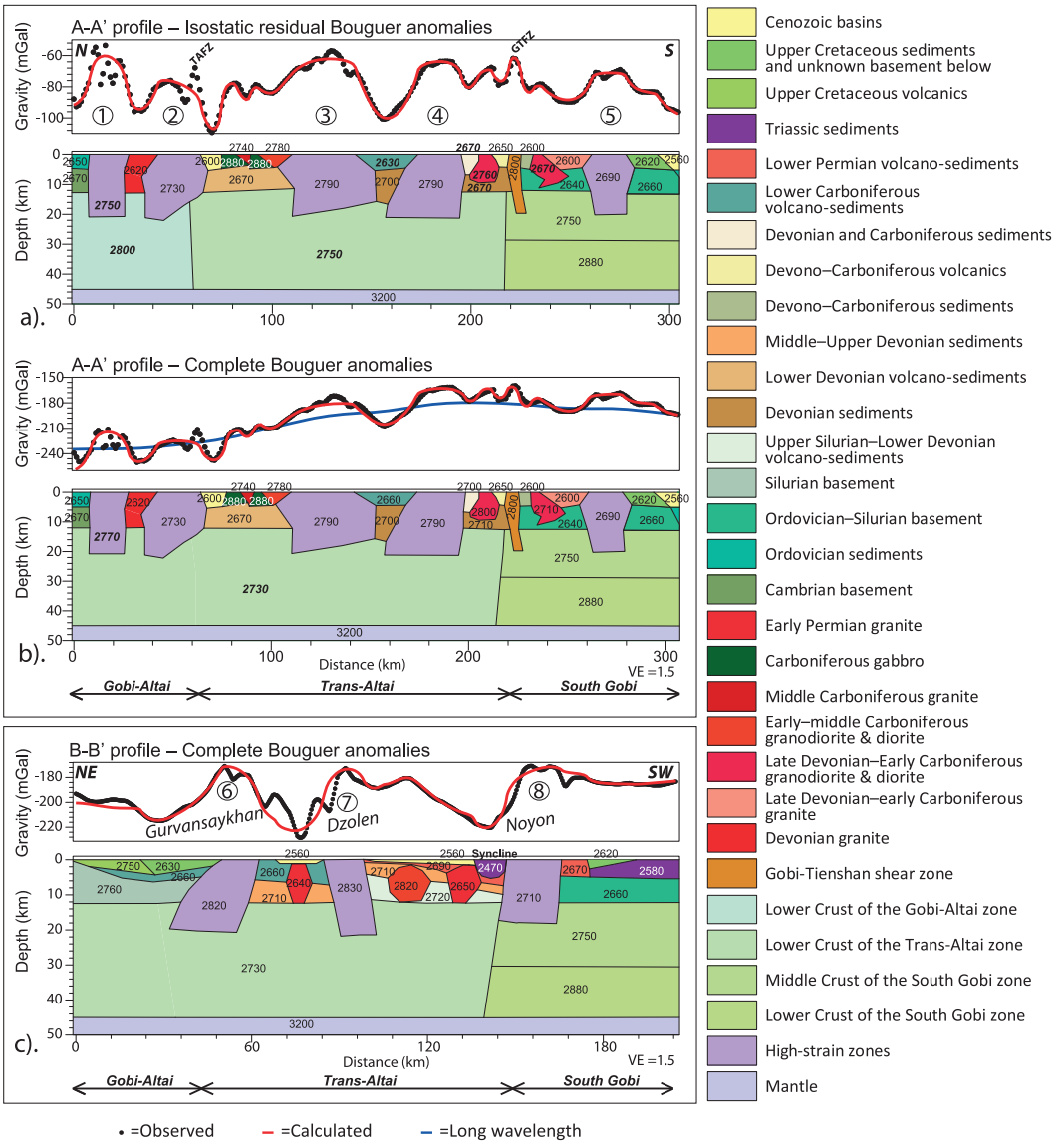

Figure 5. Gravity profiles. Gravity models of profile A-A' across southwestern Mongolia. (a) Isostatic residual Bouguer gravity anomaly model. (b) Complete Bouguer gravity anomaly model. (c) Complete Bouguer gravity anomaly model of profile B-B' across central southern Mongolia. The numbers are the density values in kg/m^3, and the bold numbers underline the density values which needed to be changed to satisfy the Bouguer gravity anomaly. (1) Lower Devonian sediments and Mid-Ordovician granodiorite. (2) Upper Riphean volcanic rocks. (3) Lower Devonian sediments, Lower Carboniferous sediments, and granodiorite. (4) Lower Devonian, Lower Carboniferous, and Upper Devonian–Lower Carboniferous sediments. (5) Lower Carboniferous volcanic rocks. (6 and 7) Upper Silurian–Lower Devonian sediments with ultramafic rocks, and Lower Devonian and Carboniferous sediments with Permian volcano-sedimentary sequences. (8) Carboniferous and Permian volcano-sedimentary sequences. TAFZ: Trans-Altai fault zone; GTFZ: Gobi-Tianshan fault zone.

3.3. Results of Gravity Modelling

3.3.1. Profile A-A'

The NNE-SSW trending profile A-A' is 305 km long. It is located in southwestern Mongolia and crosses the Gobi-Altai, Trans-Altai, and South Gobi zones (Figure 3). The position of this profile has been chosen because of the alternation of high- and low-strain zones affecting all the tectonic domains typical of southern Mongolia including accretionary wedge, continental, and oceanic domains. In addition, the modelling has been performed to investigate the relationship and the density contrasts between the lower crust of the Gobi-Altai and Trans-Altai domains.

The complete Bouguer gravity anomalies of the profile A-A′ range from approximately −240 mGal in the north to approximately −180 mGal in the south and are marked by five intermediate-wavelength and several secondary short-wavelength anomalies which can be better distinguished using the isostatic residual anomalies (Figure 5a). The upper and middle crusts are modelled as laterally variable vertical density units corresponding to the regional distribution of high-strain (correlating with intermediate wavelength gravity highs) and low-strain zones delineated at the surface [*Lehmann et al.*, 2010; *Leonov*, 2012; *Guy et al.*, 2014a]. The compositions of the high-strain zones vary from Upper Riphean volcanic rocks through Ordovician granodiorites to Lower Carboniferous sediments. Therefore, their densities contrast and it is likely that their shapes and thicknesses impact on the gravity signal. For this reason, the high-strain zone rocks have been assigned density values between 2690 kg/m^3 and 2790 kg/m^3 in our model. The gravity signal characteristically reflects the steepening of all lithologies along vertical deformation zones [*Guy et al.,* 2014a, 2014b], thus implying that the high-strain zones form tabular bodies deeply rooted in the crust (Figure 5b).

The low-strain zones are subdivided into blocks composed of Paleozoic volcanic and sedimentary sequences, Mesozoic and Cenozoic basins. Short-wavelength anomalies spatially correlate with large magmatic bodies (gabbro, granodiorite, and granite) and the Gobi-Tianshan and Trans-Altai fault zones. The Devonian granite in the Gobi-Altai Zone and the Late Devonian–Early Carboniferous granite in the South Gobi Zone correspond to gravity lows and were modelled as leucogranites with densities of 2620 kg/m^3 and 2600 kg/m^3, respectively. The Late Devonian–Early Carboniferous intrusions located at the boundary between the Trans-Altai and Gobi-Altai zones correspond to gravity highs and were modelled as diorite with density of 2800 kg/m^3 and granodiorite with density 2710 kg/m^3. A density ranging from 2560 to 2620 kg/m^3 was assumed for the Mesozoic and Cenozoic basins.

The long wavelength gradient is modelled as the variation of the densities in the lower crust since the Moho depth is considered roughly constant in southern Mongolia (Figure 4). Application of *Rudnick and Fountain's* [1995] assumption that the density increases with depth would lead to an unrealistic density distribution of the upper crustal bodies for the Mongolian tract of the CAOB. Therefore, in order to fit the observed and calculated gravity anomalies, different density values have to be invoked for deep crustal levels. Moreover, without changing the shapes and the densities of the upper crustal bodies, the modelling shows that the main difference between the isostatic residual model and the Bouguer anomaly model is a decrease in density of the Gobi-Altai lower crust (Figures 5a and 5b). The main result of this model is that the lower crust underneath the Gobi-Altai and Trans-Altai zones is geophysically homogeneous and characterized by a significantly lower density of 2730 kg/m^3 compared to the adjacent South Gobi Zone which shows a standard layered distribution of lower crustal densities.

3.3.2. Profile B-B′

Profile B-B′ located in southern Mongolia is 210 km long and trends NE-SW from the southern part of the Gobi-Altai Zone across the Trans-Altai Zone to the South Gobi Zone (Figure 5c). The location of this profile has been chosen because it crosses another typical region in which high- and low-strain zones alternate, and therefore, a comparison can be made between the architecture and density of the lower crust in this profile with that of profile A-A′.

The complete Bouguer gravity anomalies along the profile B-B′ range from −172 mGal to −228 mGal and are marked by three intermediate and several secondary shorter wavelength anomalies. In the case of profile A-A′, the intermediate-wavelength gravity highs coincide with the boundaries of major high-strain zones. According to the surface geology, the lithologies of the Gurvansaykhan and the Dzolen high-strain zones are comparable but differ from that of Noyon. The compositions of the rocks vary from Upper Silurian–Lower Devonian sediments for the Gurvansaykhan and Dzolen zones to Carboniferous and Permian volcano-sedimentary sequences for the Noyon Zone. Moreover, the presence of numerous lenses of ultramafic rocks in the Gurvansaykhan and Dzolen zones makes them significantly denser than the high-strain zones in the profile A-A′. Therefore, the zones have been assigned density values of 2820 kg/m^3 and 2830 kg/m^3, respectively, whereas a density of 2710 kg/m^3 has been attributed to the Noyon high-strain zone. As in the case of profile A-A′, the high-strain zones can be modeled as tabular and steeply inclined bodies deeply rooted in the crust (Figure 5c).

The low-strain zones are subdivided into blocks consisting of Paleozoic volcanic and sedimentary sequences intruded by Early Permian granites and Early-Middle Carboniferous granodiorite and diorite on the one hand, and by Mesozoic and Cenozoic basins on the other hand. The wide Cretaceous basin in the Gobi-Altai Zone

coincides with a gravity gradient which is linked to the presence of a major Early Cretaceous basaltic field juxtaposed against Late Cretaceous sediments. Between the Gurvansaykhan and the Dzolen high-strain zones, high-frequency variations in the gravity anomaly are superimposed on a long-wavelength gravity low. This area is covered by Cenozoic sediments but the presence of Early Permian granite with a density of 2640 kg/m^3 was extrapolated from the south onto our profile. To the north-west and to the south-east of the profile, Early-Middle Carboniferous granodiorite and diorite intruded the Middle–Upper Devonian sediments. Thus, by transposition, the gravity high of the Cenozoic basin located between the Gurvansaykhan and the Noyon high-strain zones was interpreted as Early-Middle Carboniferous granodiorite and diorite, and this body was assigned a density of 2820 kg/m^3. The Noyon Uul syncline is assumed to reach ~5 km in depth and is composed of Triassic fluviatile sediments [*Dumitru and Hendrix*, 2001; *Guy et al.*, 2014a]. It coincides with a gravity low and was assigned a density of 2470 kg/m^3. However, the modelling of the syncline itself did not succeed in fitting the observed gravity anomaly to the calculated one. Therefore, the presence of Early Permian granite with a density of 2650 kg/m^3 was assumed as these occur on both sides of the profile.

Finally, the long-wavelength anomalies were modelled as the variation of the densities in the lower crust. As in the profile A-A′, a lower density of 2730 kg/m^3 was attributed to the lower crust compared to the bulk of the upper crust along profile B-B′. Also, as in the profile A-A′, the anomalously low density of the lower crust underneath the Trans-Altai Zone contrasts to a standard distribution of lower crustal densities underneath the South Gobi Zone.

4. Composition of the Lower Crust as Constrained by Granitoid Petrology and Whole-Rock Geochemistry

A powerful tool used to constrain the composition of the deep crust and its development over time is the geochemistry of granitoids intruding the main geotectonic units [*Jahn*, 2004; *Kröner et al.*, 2014]. In the current study we used unpublished, geospatially referenced data on major and trace element geochemistry, SHRIMP zircon U-Pb ages, and in situ Hf isotopic compositions of dated zircons (see Appendix A for the techniques of analysis). These data were obtained as the result of an extensive survey carried out by CERCAMS along two sections orthogonal to the main tectonic boundaries of southern Mongolia [*Armstrong et al.*, 2010].

Granitoid rocks were analyzed in order to provide information about their compositions, ages of crystallization and sources. Emphasis was placed on largely unaltered samples of Carboniferous to Permian (350–250 Ma) granitoids intruding the oceanic crust domain of the Gobi-Altai and the Trans-Altai zones. They can be subdivided into two suites, an older subalkaline (OG) and a younger alkaline (YG). While the OG suite occurs in both the Gobi-Altai and Trans-Altai zones, the YG suite is known only in the Trans-Altai Zone [*Yarmolyuk et al.*, 2012].

In the multicationic R_1-R_2 plot [*De La Roche et al.*, 1980] (Figure 6a), the analyses of the OG suite clusters mainly in the fields of (subalkaline) granite-granodiorite, but a few samples spread into the adjacent fields of quartz syenite, tonalite, and diorite/gabbrodiorite. The YG form a distinct group of seven alkali granites. The B-A diagram [*Debon and Le Fort*, 1983; *Villaseca et al.*, 1998] (Figure 6b) denotes the relationship between the contents of dark minerals and alumina saturation and, consequently, the characteristic mineral assemblage. The analyses are, with a single exception, metaluminous to subaluminous and plot along two trend lines reflecting the modal compositions of OG and YG, respectively. The trend for the subalkaline OG corresponds to biotite-amphibole bearing assemblages, while that of the alkaline YG is typical of an amphibole-dominated suite. The only outlier is T1-191 which is a strongly peraluminous leucogranite.

Most of the studied granitoids from the Gobi-Altai and Trans-Altai zones correspond to high-K calc-alkaline associations, with some straddling the boundary of the adjacent shoshonitic field [*Peccerillo and Taylor*, 1976] (Figure 6c). On average, rocks of the alkaline YG suite show a particularly potassium-rich composition. In addition, they have typical features of A-type magmas, such as an enrichment in HFSE (in particular high Ga/Al) and high FeOt/MgO ratios (Figure 6d) [*Eby*, 1990; *Whalen et al.*, 1987]. On the other hand, the OG samples have an overall I-type affinity, and plot accordingly into the "I & S" field of the 10000Ga/Al versus FeOt/MgO plot.

Average lower crust-normalized spiderplots [*Taylor and McLennan*, 1995] reveal some important differences between the two suites. The OG suite mostly shows a coherent behavior, with normalized trace element

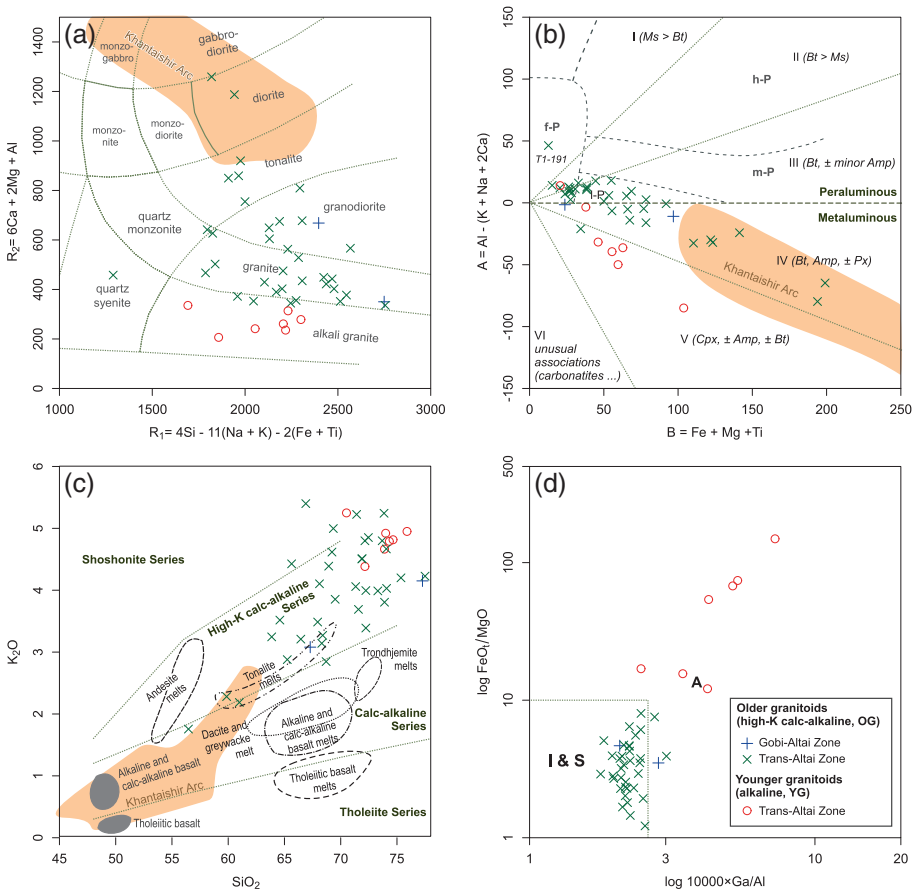

Figure 6. Classification of the studied Carboniferous-Permian granitoid rocks from the Gobi-Altai and Trans-Altai zones. (a) Multicationic diagram R_1–R_2 [*De La Roche et al.*, 1980]. (b) B–A multicationic plot of *Debon and Le Fort* [1983, modified by *Villaseca et al.*, 1998]. I-P: low peraluminous, m-P: moderately peraluminous, h-P: highly peraluminous, f-P: felsic peraluminous. (c) Binary plot SiO_2–K_2O [*Peccerillo and Taylor*, 1976]. The fields of experimental melts derived from various sources are taken from Figure 3 of *Roberts and Clemens* [1993]. (d) Binary plot log 10000 × Ga/Al versus log FeO_t/MgO (by weight) distinguishing A-type granites (their average marked by "A") from fractionated I and S types ("I & S") [*Whalen et al.*, 1987]. The orange field in Figures 6a–6c denotes the distribution of Cambrian plutonic rocks from the Khantaishir arc [*Janoušek et al.*, 2014, also unpublished data, 2014].

concentrations often varying only within a narrow range (Figure 7a). In comparison with average lower crust, the OG samples are enriched in LILE, in particular Cs, Rb, Th, U, and K, less so Ba. Also the contents of LREE and MREE, Zr and Hf are elevated. The normalized Nb, Ta and HREE contents are rather variable and on average not very different from unity. Lastly, Ti shows a significant depletion. Also Ba and Sr display significant negative anomalies, most likely due to the effects of feldspar fractionation.

Compared to the OG, the alkaline YG rocks are strongly enriched in Nb, Ta, and HREE (Figure 7b). Rb, LREE, MREE, Zr, and Hf are less elevated. The negative anomalies for Ba, Sr, and Ti are greater than in the case of the OG suite. Such high contents of alkalis, REE (except Eu), HFSE (Nb, Ta, Y, Zr, and Ga), combined with low contents of the trace elements behaving compatibly in feldspars (Ba, Sr, Eu) are a hallmark of within-plate, A-type igneous activity [*Bonin*, 2007; *Eby*, 1990; *Whalen et al.*, 1987] and indeed the YG suite plots in the Within-Plate Granite field of *Pearce et al.* [1984] (not shown).

5. Discussion

The Mongolian CAOB is traditionally interpreted as a collage of numerous accreted terranes [*Badarch et al.*, 2002]. *Kröner et al.* [2010] assigned these to five large tectonic zones of contrasting origins. They can be interpreted, from north to south, as cratonic, Neoproterozoic accretionary wedge, Devonian passive margin established on Late Cambrian accretionary wedge, Siluro-Devonian oceanic and, again, cratonic

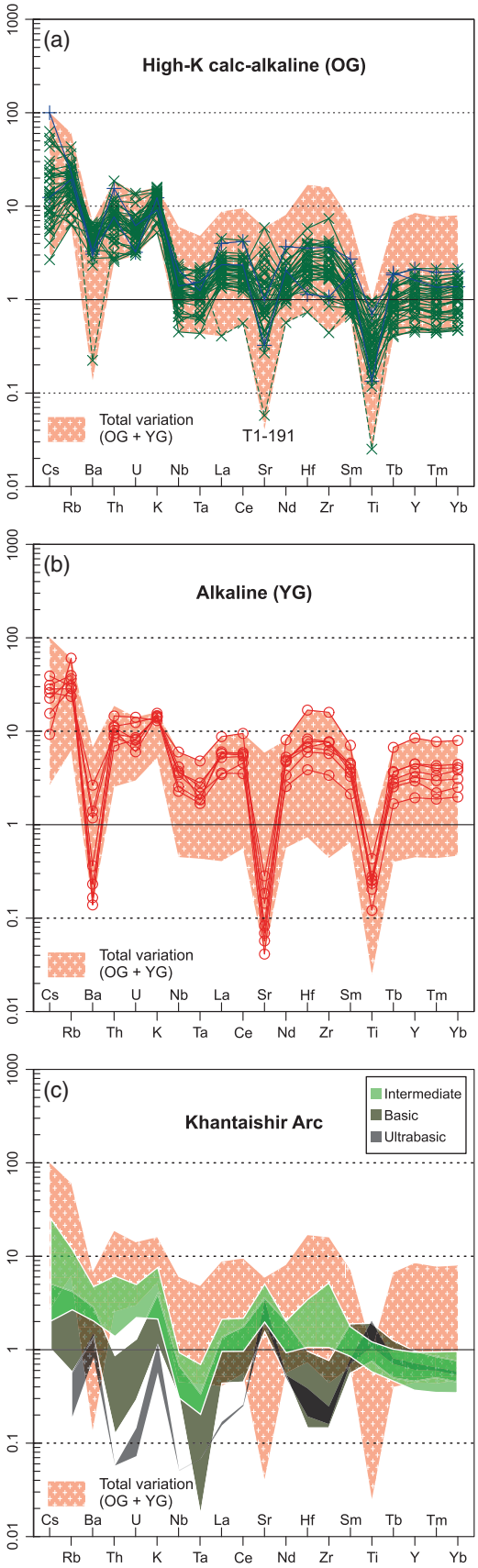

zones (Figure 1). In theory, these tectonic zones should exhibit contrasting geophysical signatures and should be limited by vertical tectonic boundaries down to the Moho as has been shown in similar accretionary systems of Alaska and eastern Australia [*Glen et al.*, 2007; *Burton*, 2010]. The study of *Guy et al.* [2014b] and this work show that this is not the case in southern Mongolia where the Paleozoic oceanic and accretionary systems are underlain by a thick homogeneous lower crust of unknown origin. The geophysical pattern, composition, and likely petrological character of this enigmatic lower crust are discussed below.

5.1. Thickness of the Crust of the Trans-Altai Zone

According to seismic studies, the crust of the Trans-Altai oceanic zone is 45 km thick (Figure 4). The predominance of oceanic rocks at the surface however implies relatively thin crust (~30 km) such as typical oceanic arcs [*Holbrook et al.*, 1999; *Spakman and Hall*, 2010], accretionary wedges [*Moore et al.*, 1991; *Glen et al.*, 2007], or back-arc domains (which can be even thinner) [e.g., *Sato et al.*, 2014]. The only exceptions are the oceanic plateaux under which the crust can reach a thickness of 45 km [e.g., *Saunders et al.*, 1996; *Veenstra et al.*, 2006]. However, the oceanic plateaux are characterized by Large Igneous Province chemistry of their basaltic volcanic rocks [*Arndt et al.*, 2001], which is not the case for the studied area. Magmatic rocks of the Trans-Altai Zone are generally andesitic basalts, dacites, and tonalites formed in an arc-type environment together with classical tholeiitic basalts or gabbros which are believed to have formed in back arcs [*Lamb and Badarch*, 2001; *Helo et al.*, 2006].

It is well-known that the oceanic segments in this area are imbricated [*Zonenshain*, 1973; *Suyetenko et al.*, 1988] during Late Devonian convergence [*Ruzhentsev et al.*, 1992] forming so-called "intraoceanic ophiolites" [*Şengör and Natal'in*, 1996]. If the oceanic crust was tectonically imbricated to reach a total thickness of 45 km, then the resulting pile would be composed of an exceptionally high-density material and would create a large-scale positive gravity

Figure 7. (a–b) Average lower crust [*Taylor and McLennan*, 1995] normalized spiderplots for the two studied granitoid suites. The background field portrays the overall variation in the whole data set. Symbols are as in Figure 6. (c) Fields denoting normalized compositions (the same norm and scale) of ultrabasic ($SiO_2 < 42$), basic ($42 < SiO_2 < 52$ wt %) and intermediate ($SiO_2 > 52$ wt %) plutonic rocks from the Khantaishir arc [*Janoušek et al.*, 2014, also unpublished data, 2014].

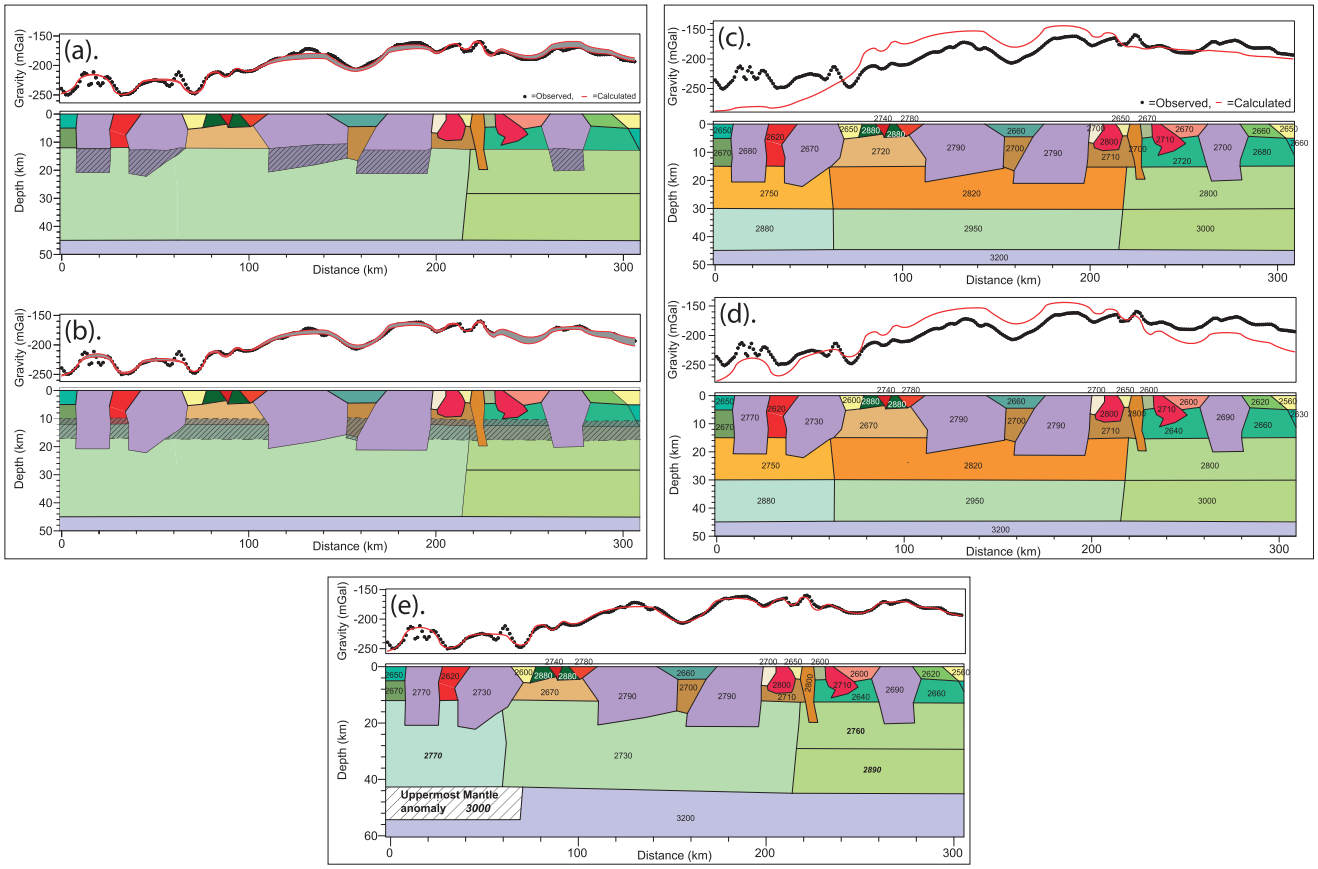

Figure 8. Geometry and density sensitivity tests of profile A-A′ of the Bouguer gravity anomaly. The sensitivity of the model to the three principal crustal layers is also tested. (a) Calculated gravity resulting from the decrease of depth of the high-strain zones from 21 to 16 km. (b) Calculated gravity resulting from the variation of the thickness of the upper crust from 12 to 17 km depth and from 12 to 9 km. Grey-shaded areas indicate the variation in the gravity responses; striped areas indicate the modification of the structures. (c) Calculated gravity resulting from the model where three crustal layers and the average density values of models are assumed. (d) Calculated gravity resulting from the model where the average density values of the lower and middle crusts come from the crustal models of *Rudnick and Fountain* [1995] and *Christensen and Mooney* [1995], and the density values of the upper crust are based on our model. (e) Complete Bouguer gravity anomaly model with the mantle anomaly hypothesis described by *Petit et al.* [2002] and the density values of the upper crust coming from our model. (f) Our model.

anomaly over the entire Trans-Altai Zone and possibly also the Gobi-Altai Zone. However, the gravity modelling (Figures 5b and 5c) shows that the lower crust is intermediate to felsic and homogeneous underneath the Gobi-Altai and the Trans-Altai zones.

5.2. Tests of the Architecture and Density Distribution of the Crustal Structures of the South Mongolian CAOB

Forward modelling of gravity anomalies is a quantitative method, but its application is limited by the nonuniqueness of the results as many different models can be elaborated to fit the observed data. Although the geological, geochemical, petrophysical, and seismic constraints are essential to reduce these ambiguities associated with gravity analysis, geometry and density sensitivity tests (Figure 8) for our forward models (Figure 5) have to be performed to assess the relative influence of the variations in the crustal architecture and the density contrasts on the gravity responses. When the model is very sensitive to geometry or density changes, it means that our model is the most probable of the crustal architecture.

To undertake the geometry sensitivity test, the density values of the different structures were fixed in order to assess the effects of varying the high-strain zone geometry and the depth of the upper crust (Figures 8a and 8b). To begin the process of constructing the density model, the high-strain zones were assumed to be roughly rectangular, steeply dipping bodies and the model was then adapted in order to fit the observed gravity anomalies. The geometrical sensitivity of the model with respect of thickness of the high-strain zones was tested by varying their thickness from 21 km to 16 km (Figure 8a). The gravity response to the

decrease of thickness is weak in the Gobi-Altai Zone, whereas it decreases in the Trans-Altai and increases in the South Gobi zones, respectively (gradient of ~4 mGal/km). Thus, the high-strain zones are most probably rooted deeply to ~20 km depth in the Trans-Altai and South Gobi zones but are probably shallower in the Gobi-Altai Zone. Finally, the geometrical sensitivity of the model with regard to the thickness of the upper crust was tested by increasing its thickness from 12 to 17 km depth and by decreasing it from 12 to 9 km (Figure 8b). In both cases, the test shows that the gravity response is weakly sensitive for the Gobi-Altai Zone, where a gradient of ~0.3 mGal/km is observed, but is more sensitive for the Trans-Altai and South Gobi zones where a gradient of 2 mGal/km is present. Therefore, a thickness of 12 km for the upper crust seems reasonable for the purpose of modelling.

To undertake the density sensitivity test, the geometry of the upper crustal structures was maintained in order to assess the influence of varying the density contrasts in the deepest part of the crust (Figures 8c and 8d). In addition, we tested the three-layered crustal model and the increase of the density values with depth according to the models of *Rudnick and Fountain* [1995] and *Christensen and Mooney* [1995]. Firstly, the sensitivity of the model to the variation of the density contrasts was tested by entering the characteristic average density values of each crustal type established by the two studies cited above (Figure 8c). This analysis shows that the crustal models of these authors are not applicable to southern Mongolia. In order to test the influence of the density contrasts of the upper crust, a second test was run, in which the density values of the lower and middle crusts are taken from the work of *Rudnick and Fountain* [1995] and *Christensen and Mooney* [1995], and the densities of the upper crust remain the same as those used in our model (Figure 8d). This analysis shows that the density distribution required to satisfy the gravity anomaly would be consistent neither with the defined lithologies of the tectonic zones nor with the types of crust defined by *Rudnick and Fountain* [1995] and *Christensen and Mooney* [1995]. For example, locally a density of up to 2900 kg/m^3 for sedimentary sequences would be required. Therefore, these two tests demonstrate that the gravity anomalies cannot be explained by a progressive increase of densities with depth.

The third test on the profile A-A′ (Figure 8e) was made to investigate the hypothesis of a low-density uppermost mantle anomaly in the Hangay region [*Petit et al.*, 2002] which would extend underneath the Gobi-Altai Zone. Their mantle anomaly was modelled as a 10 km thick prism with a density contrast of −200 kg/m^3 compared to the surrounding mantle located at a depth range 50–60 km. In our model, the uppermost mantle anomaly has the same shape and density contrast. This mantle anomaly model shows that the regional gravity anomaly can be modelled using the same upper crustal density distribution and three contrasting density values in the lower crust. Moreover, in order to fit the calculated with the observed gravity profiles, the mantle anomaly has to be located at a depth between 43 and 53 km which moves the topography of the Moho to a slightly shallower depth. In addition, the lower crustal densities of the Trans-Altai and the Gobi-Altai zones, even if they differ, are still too low for typical lower crustal values [*Christensen and Mooney,* 1995]. Therefore, our model does not necessarily exclude the presence of an upper mantle anomaly in the northern part of southern Mongolia similar to the one underlying the Hangay region [*Petit et al.,* 2002].

This study shows that between the upper crustal and mantle layers, a zone with a homogeneous long-wavelength signal in which the terrane boundaries cannot be delineated is present. In contrast to the model of *Rudnick and Fountain* [1995], the forward modelling implies that this layer cannot be composed of dense lower crustal material, such as gabbro or mafic granulite (Figure 5). Assuming that our model provides the correct distribution of densities and architecture of the upper crust in the Gobi-Altai and Trans-Altai zones, the underlying lower crust has to be intermediate to felsic in composition. The main question then arises. What is the nature of such a geophysically anomalous lower crust?

5.3. Composition and Origin of the Lower Crust

The majority of continental granitic plutons are thought to have been produced by dehydration melting of three hydrous mineral phases, muscovite, biotite, and amphibole [*Clemens,* 2012, and references therein]. Even though the role of water-fluxed melting may have been underestimated [*Weinberg and Hasalová,* 2015], several main types of fertile sources of granitic magmas can be distinguished on geochemical grounds: (1) pelitic (clay-rich, feldspars-poor, producing geochemically mature, strongly peraluminous granites with high Rb/Sr, Rb/Ba and low CaO/Na_2O ratios), (2) quartzo-feldspathic (clay-poor and feldspars-rich orthogneisses or greywackes, yielding mainly subaluminous or metaluminous, granitic magmas with low Rb/Sr, Rb/Ba and high CaO/Na_2O ratios), and (3) metabasic (amphibole-bearing, giving typically

geochemically rather primitive, metaluminous, I-type tonalites to trondhjemites, or granodiorites to granites) [e.g., *Harris and Inger*, 1992*; Johannes and Holtz*, 1996*; Patiño Douce and McCarthy*, 1998; *Clemens,* 2012].

Information on the composition of the lower crust in the south Mongolian CAOB in Carboniferous times is provided by inferred sources of the high-K calc-alkaline granitic magmas of the OG suite. The binary plot $Al_2O_3 + FeOt + MgO + TiO_2$ versus $Al_2O_3/(FeOt + MgO + TiO_2)$ proved useful in discriminating the possible sources of granites [*Jung et al.*, 2009; *Janoušek et al.*, 2010] (Figure 9a). The OG samples plot in the fields of melts derived from quartzo-feldspathic sources, i.e., orthogneiss or greywacke, and metabasite (amphibolite). In this case a pelitic parentage can be ruled out. This is also in line with the subaluminous to metaluminous nature of most of the studied granitoids. Accordingly, low Rb concentrations relative to Sr and Ba suggest a clay-poor source (Figure 9b). Taken together, a metapelitic parentage can be excluded with confidence for all samples, apart from the peraluminous leucogranite T1-191.

Moreover, as shown by *Roberts and Clemens* [1993] and *Clemens* [2012], the high-K calc-alkaline rocks similar to the OG suite cannot be generated by partial melting of tholeiitic or calc-alkaline basalts (Figure 6c). Instead, hydrous, arc-related (calc-alkaline or high-K calc-alkaline) intermediate (andesitic or tonalitic) sources are required. Subsequently, the magma probably evolved by substantial fractional crystallization. Still, as shown by *Roberts and Clemens* [1993], such fractionation would not shift the magma composition outside the given high-K calc-alkaline field (Figure 6c).

Direct information on the crustal residence age and geochemical character of the sources comes from integrated U-Pb ages and Hf-isotope information for zircons from Carboniferous granitoids (OG suite) intruding the Gobi-Altai and Trans-Altai zones (Figure 9c). The relatively young model ages for the granitoids in the Trans-Altai Zone (0.63 ± 0.12 Ga) rule out any major involvement of Grenvillean material (or older) that occurs in the South Gobi Zone to the south [*Yarmolyuk et al.*, 2007; *Rojas-Agramonte et al.*, 2011] and the Baydrag Continent to the north [*Kröner et al.*, 2014].

Instead, the zircon population is dominated by a juvenile component, as indicated by strongly positive initial ε_{Hf} values (Gobi-Altai Zone: $+9.8 \pm 0.9$, Trans-Altai Zone: $+12.4 \pm 0.6$; median $\pm 1\sigma$) and low two-stage Hf model ages (Gobi-Altai Zone: 0.89 ± 0.14 Ga, Trans-Altai Zone: 0.63 ± 0.12 Ga) (Figure 9c). These data can be explained in two ways. The first possibility is direct derivation during the Carboniferous from a mantle somewhat less depleted than the model MORB–DM reservoir in Figure 9c. However, the field relations, petrology, and the outstanding whole-rock geochemical signature clearly rule out a mantle parentage. Were these mostly granitic plutons a result of extensive fractionation of mantle-derived, basaltic magmas, one would expect to encounter large volumes of (ultra)mafic cumulates and increasingly rarer products of the magma differentiation. The present level of erosion is characterized by voluminous acid intrusions and a relative scarcity of intermediate to basic magmatic rocks. The presence of such dense cumulate rocks, even deep in the lower crust, would certainly have been detected in our gravimetric modelling.

The second scenario is that the studied granitoids originated from partial melting of a fairly primitive and young heterogeneous intermediate ($\gg$ basic) lower crust. A possible candidate is the Neoproterozoic accretionary wedge and ophiolites of the Lake Zone [*Zonenshain and Kuzmin*, 1978] thrust over the Baydrag Continent during the Early to Late Cambrian [*Štípská et al.*, 2010; *Jian et al.*, 2014]. The material of the Trans-Altai Zone is exclusively of oceanic origin and thus fairly juvenile [*Dijkstra et al.*, 2006; *Kröner et al.*, 2014]; however, it is too old and too mafic to be a viable source for the granites in the Trans-Altai Zone.

Nevertheless, much of the Lake Zone is made of remnants of a huge magmatic arc discovered recently in the Khantaishir and Zamtyn Nuruu mountain ranges [*Janoušek et al.*, 2014; *Hanžl et al.*, 2014]. This "Khantaishir" arc is composed of geochemically rather primitive gabbros, diorites, and (prevalent) tonalites of Cambrian age (520 to 495 Ma) (Figure 7c). The composition and age of this material make it an appropriate source for the Carboniferous and Permian Trans-Altai Zone granites (Figure 9c).

The situation of the Carboniferous Gobi-Altai Zone granites is more complex, because the data are limited and the hafnium model ages are on average higher (0.893 ± 0.137 Ga). This may be due to the significant proportion of Grenvillean material coming either from the Lake Zone or the Baydrag Continent [*Demoux et al.*, 2009; *Yarmolyuk et al.*, 2013; *Kröner et al.*, 2014].

Taken together, a viable scenario for the genesis of the Carboniferous high-K calc-alkaline suite (OG) would be the anatexis of a metaigneous lower crust (tonalite $\gg$ diorite and gabbro). As shown by experiments

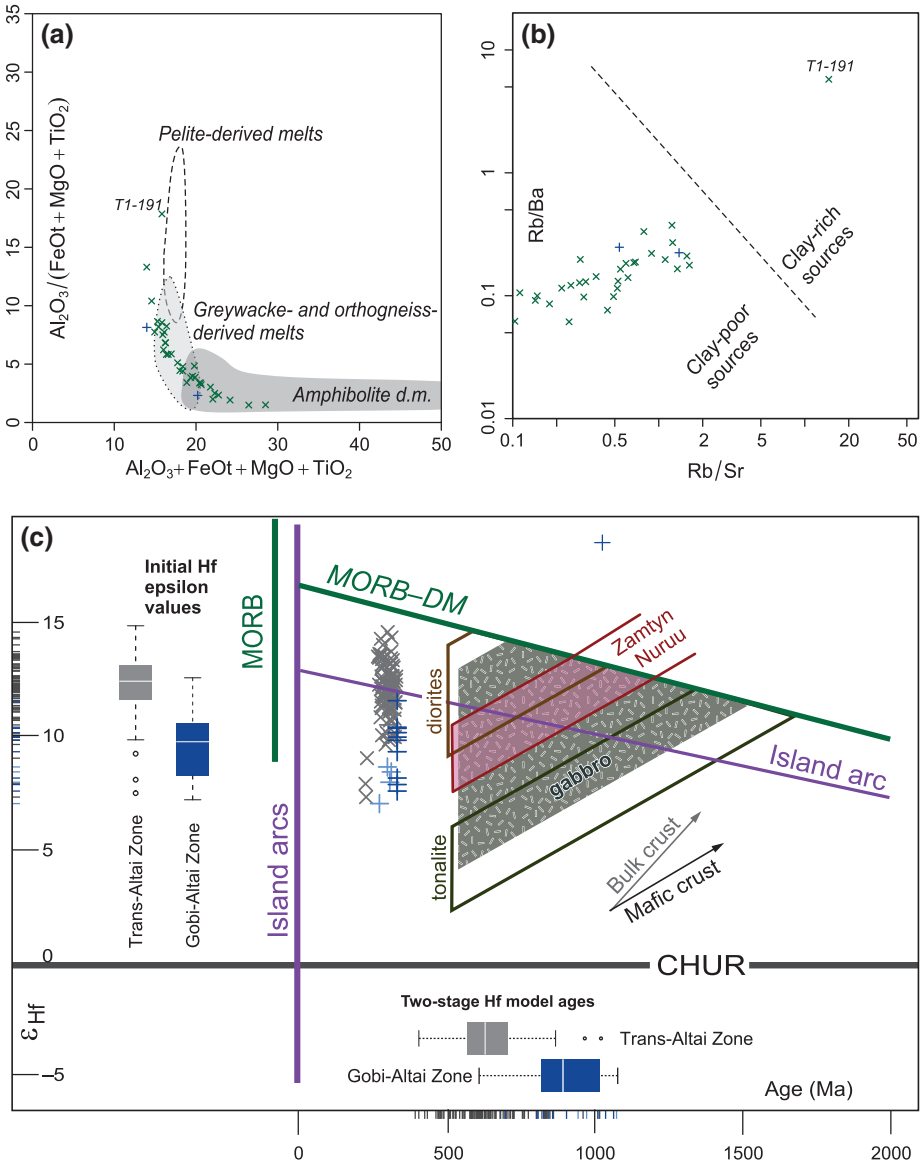

Figure 9. (a) Binary plot $Al_2O_3 + FeO_t + MgO + TiO_2$ versus $Al_2O_3/(FeO_t + MgO + TiO_2)$ for older granites; outlined are domains occupied by experimental granitic melts obtained by partial melting of metapelites, metagreywackes, and amphibolites [*Janoušek et al.*, 2010, and references therein]. (b) Diagram of Rb/Sr versus Rb/Ba after *Sylvester* [1998] underlining the fact that the nearly all studied rocks are unlikely to come from anatexis of clay-rich (pelitic) metasediments. Symbols are as in Figure 6. (c) Two-stage Hf development diagram for zircon from plutonic rocks of the Gobi-Altai Zone (blue) and Trans-Altai Zone (dark gray) (database of CERCAMS and unpublished data of P. Hanžl for the Chandman Massif (lighter blue)). The background fields denote the variation in a tonalite, gabbro, and two diorites from the Khantaishir arc [*Janoušek et al.*, 2014, Y. Jiang, unpublished data, 2014] and Zamtyn Nuruu arc further east (pink field) (P. Hanžl, unpublished data, 2014). The average basaltic $^{176}Lu/^{177}Hf$ for the two-stage growth model is assumed to be 0.022 [*Lancaster et al.*, 2011]. The ranges shown by modern MORB and island arcs as well as the evolution line for the mean mantle source to modern island-arc magmas are taken from the compilation of *Kemp and Hawkesworth* [2014, and references therein].

[*Skjerlie and Johnston*, 1992; *Patiňo Douce*, 1997], significantly younger (Permian), high-T, dry partial melting of a similar source could have yielded melts with geochemical characteristics of A-type granitoids, i.e., analogous to the Permian alkaline YG suite.

5.4. Thermodynamic Modelling of Khantaishir Protoliths and Lower Crustal Densities

In order to test whether the Khantaishir arc rocks can form the present lower crust underlying the Gobi-Altai and Trans-Altai zones, their petrology and density were modelled assuming tectonic emplacement under

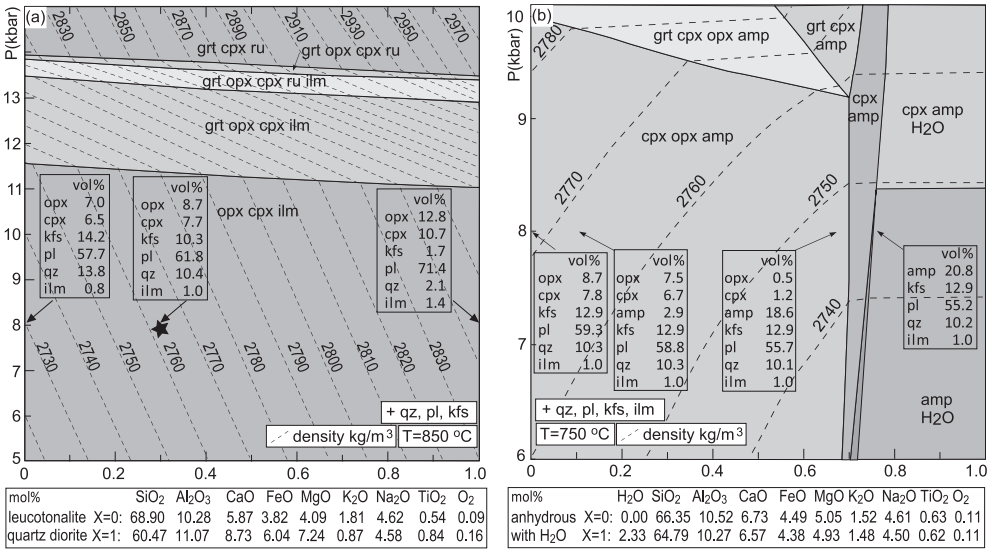

Figure 10. Pressure-composition (P-X) diagrams showing variation of mineral assemblage on pressure and whole-rock composition, contoured for density. (a) For anhydrous whole-rock compositions varying between leucotonalite and quartz diorite; (b) for increasing amount of H_2O in whole-rock composition indicated as star in (a). Used models: grt [*White et al.*, 2007], opx [*Powell and Holland*, 1999], cpx [*Green et al.*, 2007], pl-kfs [*Fuhrman and Lindsley*, 1988], ilm [*Andersen and Lindsley*, 1988].

lower crustal conditions. Calculations were carried out by Gibbs energy minimization [*Connolly*, 2005] in the Na_2O–CaO–K_2O–FeO–MgO–Al_2O_3–SiO_2–H_2O–TiO_2–O system with the database of *Holland and Powell* [1998] (Figure 10). As crustal xenoliths from Mesozoic and Cenozoic volcanics show mainly anhydrous granulite-facies assemblages [*Stosch et al.*, 1995; *Barry et al.*, 2003], temperatures of 850°C estimated from their mineral assemblages were used initially for density calculations (Figure 10a). Phase stability for pressure of 5–15 kbar is shown in a *P-X* diagram, in which the *X* axis shows the chemical variation of Khantaishir arc rocks between a leucotonalite ($X=0$) and a diorite ($X=1$). Major features include stability of opx-cpx-pl-kfs-qz-ilm for up to 11–11.5 kbar, stabilization of garnet above 11 kbar, rutile-ilmenite transition at 13–14 kbar, and orthopyroxene upper stability at 13.5–14 kbar, with all boundaries nearly independent of the whole-rock composition. The volume of individual phases varies considerably within a field; an example of a calculation is given in insets for 8 kbar. The density varies between 2720 and 2980 kg/m^3, depending on whole-rock composition and pressure, and there is an abrupt densification associated with the garnet-orthopyroxene transition. The average density of the lower crust obtained from gravity modelling is 2730 ± 20 kg/m^3 and matched best with pressures below the garnet stability field (<11 kbar), as expected for conditions of the lower crust, and for whole-rock compositions close to the modelled leucotonalite, dominated by feldspar and quartz with a maximum opx + cpx content of 17 vol % ($X=0$–0.3).

However, the Devonian-Carboniferous accretion was associated with amphibolite-facies metamorphism and only produced anhydrous assemblages sporadically [e.g., *Kozakov et al.*, 2002b; *Broussolle et al.*, 2015]. In addition, Late Carboniferous and Early Permian intrusions are localized in linear zones [e.g., *Guy et al.*, 2014b], which may imply that the Permian melting and granulitization of the lower crust were also localized processes and that the rest of the lower crust still preserved amphibolite-facies equilibria. In order to simulate the amphibolite-facies conditions, the influence of H_2O on the mineralogical assemblage and density was examined for the whole-rock composition indicated by the star in Figure 10a. The calculation is for 6–10 kbar but at a lower temperature (750°C), because upon cooling H_2O is bound in amphibole, not in the melt (Figure 10b). The *X* axis represents chemical variation between dry ($X=0$) and hydrated ($X=1$) whole-rock compositions. With an increasing amount of H_2O, the amount of amphibole increases up to 21 vol % at the H_2O saturation line (sample calculations are given as insets for 8 kbar). The conversion of pyroxenes to amphibole results in a density decrease, for example, at 8 kbar from 2772 kg/m^3 for the anhydrous assemblage to 2747 kg/m^3 for the hydrated assemblage.

Taken together, the results of petrological modelling support the view that the average composition of the lower crust in the Gobi-Altai and Trans-Altai zones is similar to that of the main rocks forming the

"Khantaishir" arc but metamorphosed at upper amphibolite- or/and granulite-facies conditions. If the lower crust is hydrated, the composition may have to be more basic to match the densities inferred from the gravity modelling.

5.5. Geodynamic Implications

Accretionary orogens form by progressive amalgamation of terranes of contrasting composition and geological history added laterally to continental nuclei [*Berg et al.*, 1972, 1978; *Coney et al.*, 1980; *Monger et al.*, 1982; *Jones et al.*, 1983]. In terms of surface geology, crustal thickness, and composition, these blocks, limited by vertical boundaries (faults or shear zones), should preserve their identities over the whole crustal column.

The geophysical and compositional characteristics of typical crustal domains such as magmatic arcs, cratons, back arcs, passive margins, and extended crust which usually make up terranes were reviewed by *Rudnick and Fountain* [1995] and *Christensen and Mooney* [1995]. This information enables reasonable prediction about the geophysical character of accreted terranes and the heterogeneity of accretionary orogens in general.

Indeed, the geophysical studies of accretionary belts like Alaska or Tasmanides showed an excellent match between geophysical signals down to the Moho and terrane boundaries, thereby confirming their identity, contrasting origins, and geological history [*Wellman*, 1988; *Glen et al.*, 2007]. The oceanic domain should display petrological and chemical heterogeneity that should also be reflected in the differences in geophysical properties as exemplified by the Wrangellia oceanic plateau in Alaska [*Glen et al.*, 2007]. In all cases, the lower crust has to be gabbroic in composition.

In contrast, there are also oceanic accretionary systems in which a lower crustal layer of distinct geophysical character is present. In such cases the composition and origin of this layer are "enigmatic" (e.g., Songpan-Ganzi accretionary orogen in northern Tibet) [*Wang et al.*, 2013]. In the Mongolian tract of the CAOB, our investigations have identified a similar enigmatic lower crust. By combining geophysical imagery, the geochemical signature of post-accretion granitoids, and thermodynamic modelling, it has been possible to constrain its nature. Using all this data, it has been concluded that the lower crust in the Mongolian tract of the CAOB consists of granulitized felsic to intermediate Cambrian arc-derived material that is clearly allochthonous with respect to the overlying Late Cambrian to Devonian oceanic crust and intra-oceanic arcs [*Lamb and Badarch*, 2001; *Helo et al.*, 2006; *Jian et al.*, 2014]. These rocks satisfy the criteria for relaminated orogenic lower crust [*Hacker et al.*, 2011; *Schulmann et al.*, 2014]; i.e., they originated elsewhere and were later emplaced tectonically into their present position. Regardless of the mechanism involved, this tectonic emplacement should have occurred before 330 Ma because that is the age of the oldest granites in the Trans-Altai Zone that sampled the relaminated material.

Based on the structural analyses of *Lehmann et al.* [2010] and *Guy et al.* [2014a], a tentative cross section depicting the Late Carboniferous to Early Permian architecture of the Mongolian CAOB is proposed. In Figure 11, the result of Early Carboniferous imbrication of the Late Cambrian to Devonian Trans-Altai oceanic crust responsible for the formation of ophiolitic nappes is shown [*Zonenshain et al.*, 1975; *Suyetenko et al.*, 1988; *Jian et al.*, 2014]. The Gobi-Altai Zone in the north was also affected by strong deformation associated with high-temperature metamorphism, voluminous magmatism, and the formation of crustal-scale magmatic and migmatite-granite domes [*Economos et al.*, 2008; *Lehmann et al.*, 2010]. In addition, *Lehmann et al.* [2010, Figure 17] argued for an Early Carboniferous underthrusting of the whole Lake Zone beneath the Gobi-Altai accretionary system which is also depicted in Figure 11. It is likely that this major Early Carboniferous accretionary event was responsible for emplacement of the Late Cambrian arc material underneath the Trans-Altai Zone and its relamination below the Siluro-Devonian oceanic crust. Finally, the whole system was affected by a major Permo-Triassic collisional event resulting in episodic development of wide heterogeneous deformation zones associated with upright folding [*Guy et al.*, 2014a]. The deformation zones are marked by a vertical anisotropy, thick roots, and intrusions of Late Carboniferous to Permian magmas testifying the extensive anatexis of the fairly juvenile Cambrian orogenic lower crust. The deep roots of the shear zones are responsible for the gravity anomalies shown in the idealized gravity profile (Figure 11), whereas granitoids intruding along these zones coincide with elongated magnetic highs [*Guy et al.*, 2014b]. These authors as well as the paleomagnetic study of *Edel et al.* [2014] suggested that there was only limited lateral translation along these zones, the implication being that the original thrust-related architecture of the Trans-Altai, Gobi-Altai, and Lake zones remains preserved (Figure 11).

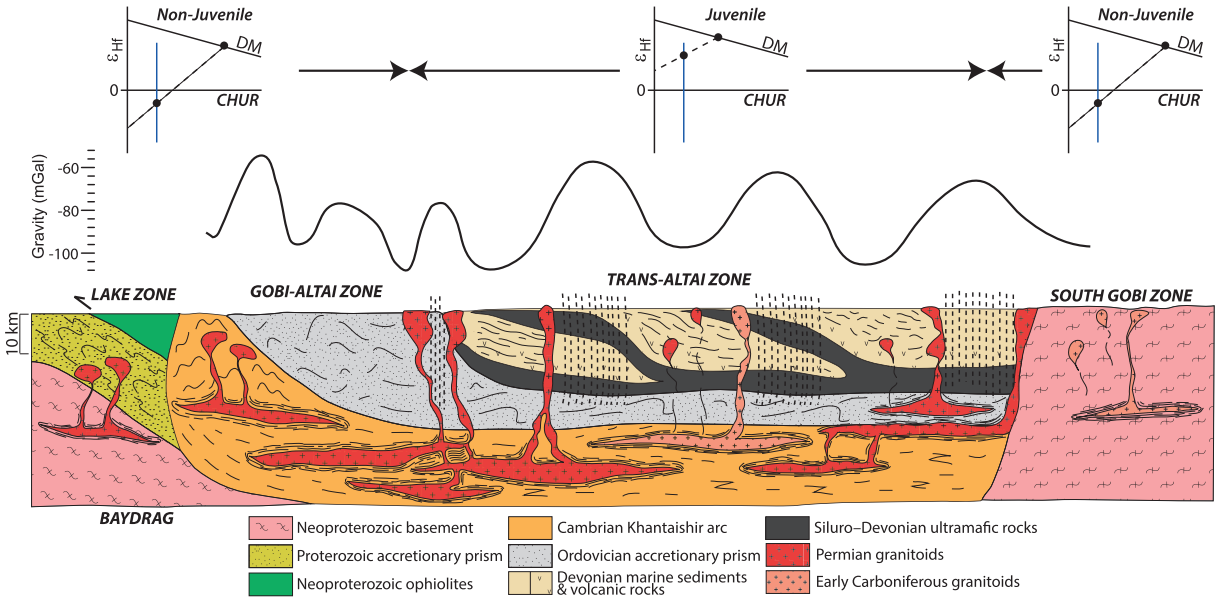

Figure 11. Permo-Triassic architecture of the southern Mongolian CAOB showing redistributed Late Cambrian Khantaishir arc material beneath the imbricated Siluro-Devonian oceanic rocks of the Trans-Altai Zone. The crustal architecture resulted from Late Devonian to Early Carboniferous accretionary tectonics. Idealized gravity profile shows nature of gravity anomalies related to steepened lithologies and thickened roots of Permo-Triassic deformation zones. The intrusions of the Permian granitoids coincide spatially with the weakened deformation zones. The top illustration shows the idealized Hf development diagrams for zircons of granitoids from individual tectonic zones. Late Carboniferous and Early Permian granites with positive ε_{Hf} values reflect the anatexis of Late Cambrian arc material relaminated below the Trans-Altai Zone. In contrast, melting of Grenvillean basement underlying the adjacent South Gobi Zone and Baydrag Continent is reflected by negative ε_{Hf} in zircon.

The likelihood that the magmatic arcs will be preserved in the geological record is fairly low [*Hawkesworth et al.*, 2010]. Their fate may vary from an entire subduction, through partial subduction/accretion to accretion depending on the arc thickness and rheology [*Boutelier et al.*, 2003]. It is important to note that thick arcs (up to 26 km thick) may be scraped off and accreted to the overriding plate, and because the presence of hot lower crust, they can be detached easily from the subducting plate and redistributed underneath the upper plate. The analogue models of scraping off, accretion, or partial subduction of arcs proposed by *Boutelier et al.* [2003] may well explain the remnants of the "Khantaishir" arc (similar to relics of the Kohistan arc in southern Tibet) and also relamination of felsic material underneath the upper plate [e.g., *Chemenda et al.*, 2000; *Hacker et al.*, 2011].

6. Conclusions

Geophysical investigations in southern Mongolia show that the vertical boundaries between its tectonic zones do not reach to the depth of the Moho. It is suggested that the underlying lower crust (1) is more than 20 km thick, (2) appears to be homogeneous underneath the Trans-Altai Siluro-Devonian oceanic zone and the Gobi-Altai Early Paleozoic accretionary wedge, and (3) has a low to intermediate density corresponding to that of metaigneous rocks with felsic-intermediate composition.

Geochemical study of Late Paleozoic granitic rocks has enabled to determine the character of their sources forming this enigmatic lower crust. The source rocks appear to be rather juvenile intermediate orthogneisses and granulites of Late Cambrian age.

Petrological modelling reveals that the lower crust in the Gobi-Altai and Trans-Altai zones probably consists of rocks originally formed in the northerly "Khantaishir" arc that were metamorphosed under upper amphibolite- to granulite-facies conditions.

The lower crust beneath the Trans-Altai and Gobi-Altai zones in southern Mongolia is therefore most probably a homogeneous, felsic to intermediate and fairly juvenile continental crust. The presence of such material underlying the oceanic crust with accretionary wedge is assumed to be due to relamination of the Khantaishir-like, Late Cambrian arc-derived material underneath the Siluro-Devonian oceanic crust during the Carboniferous.

Appendix A: Analytical Techniques

A.1. Whole-Rock Major and Trace Element Compositions

We used unpublished data of Centre for Russian and Central EurAsian Mineral Studies (CERCAMS) from the survey aimed at geodynamic-metallogenic reassessment, geotectonic reconstruction, and terrane correlation of the south Mongolian CAOB region. The geospatially referenced samples were collected during the CERCAMS ALTAIDS geotraverse in 2006 [*Armstrong et al.*, 2010]. All had a minimum mass of 5 kg of fresh material and came from surface exposures. Whole-rock samples were homogenized at Alex Stewart Assayers, OMAC Laboratories (Galway, Ireland) using their "P5 procedure." Approximately 1 kg was pulverized to $<100\,\mu m$ using a ceramic plate continuous feed mill. Of this homogenized sample, 330 g were taken for the ICP-AES and ICP-MS analyses at the OMAC Laboratories. A further split of 330 g was sent to VSEGEI (St. Petersburg, Russia) for ferrous/ferric determination via XRF and titration.

In order to achieve the maximum dissolution for all elements analyzed, two digestion methods were employed: (1) a lithium metaborate ($LiMBO_4$) fusion followed by HF dissolution using 50% HNO_3 and (2) a dissolution in 4 ml of 66% Aqua Regia for 90 min at 90°C. The latter methodology is effective for the base-metal elements.

The major elements (SiO_2, TiO_2, Al_2O_3, Fe_2O_3(total), MnO, MgO, CaO, Na_2O, K_2O, and P_2O_5) were determined by ICP-AES following the $LiMBO_4$-based dissolution methodology. Part of trace element analyses (Ag, As, B, Be, Bi, Cd, Co, Cu, Ge, Hg, Mo, Ni, Pb, Sb, Se, Te, Th, Tl, U, W, Zn, and Au) were carried out by ICP-MS following the Aqua Regia digestion. The remaining trace elements (Ba, Co, Cr, Cs, Ga, Hf, Nb, Ni, Rb, Sc, Sn, Sr, Ta, Th, U, V, W, Y, Zr, and the REE) were analyzed by ICP-MS following the $LiMBO_4$-based dissolution. Loss on ignition at 1000°C was determined by gravimetric methods. Analytical uncertainties for major and trace elements were generally better than 5%. Reproducibility and accuracy of the OMAC sample suite are well within 10%.

For the current paper we selected only Carboniferous and Permian granitoids from the Gobi-Altai and Trans-Altai zones. The analyses were further screened for effects of hydrothermal alteration or weathering ($SiO_2 < 80$ and LOI < 4 wt %) as well as the overall quality ($102 >$ Total > 98 wt %). The recalculation and plotting were done using the R language freeware package *GCDkit* [*Janoušek et al.*, 2006].

A.2. SHRIMP U-Pb Dating of Zircons

The in situ U-Pb dating of igneous zircons was performed on the Sensitive High-Resolution Ion-Microprobe (SHRIMP II) of the Centre of Isotopic Research of VSEGEI St. Petersburg (Russia). The analytical techniques are detailed in *Seltmann et al.* [2011].

The zircons were separated from 1.5–2.0 kg of the crushed material using standard VSEGEI procedure. Zircon grains were handpicked, mounted in epoxy resin together with the zircon 91500 chips, sectioned approximately in half and polished. Prior to analysis, the grains were investigated optically (in transmitted and reflected light) and studied using cathodoluminescence (CL) and backscattered electron (BSE) imaging techniques.

Each U-Th-Pb analysis consisted of four scans through the mass range. Spot diameter was approximately 20 μm, and primary beam intensity approximately 4 nA. The data were reduced broadly following the methods of *Williams* [1998, and references therein], using the SQUID Excel Macro of *Ludwig* [2000]. The calibration of the raw data was based on the analyses of the zircon 91500 (1065 Ma) [*Wiedenbeck et al.*, 1995]. The two-stage lead-development model of *Stacey and Kramers* [1975] was used for corrections of common Pb using the ^{204}Pb isotope. Uncertainties given for individual analyses (ratios and ages) are 1σ, but the concordia ages are reported at 2σ level. The concordia plots have been done using ISOPLOT/EX [*Ludwig*, 1999].

A.3. Zircon In Situ Hf Isotopic Composition

Hafnium isotope analyses were conducted using a New Wave/Merchantek LUV213 laser-ablation microprobe, attached to a Nu Plasma Multi-Collector Inductively Coupled Plasma Mass Spectrometer (LA-MC-ICPMS). The analytical spots were located over the pits from the SHRIMP analyses, so both U-Pb age and Hf-isotope data were collected from the same zircon domain. The analyses employed a beam

diameter of approximately 40 μm, a 5 Hz repetition rate, and energies of 0.6–1.3 mJ per pulse. This resulted in ablation pits typically 40–60 μm deep during a 30–120 s analysis. Total Hf signals were between 1×10^{-11} and 6×10^{-11} A. The ablated sample material was transported from the laser cell to the ICP-MS torch by a He carrier gas. Interference of ^{176}Lu on ^{176}Hf was corrected by measurement of interference-free ^{175}Lu and using the ^{176}Lu/^{175}Lu ratio of 0.02669 [*DeBievre and Taylor*, 1993]. The interference of ^{176}Yb on ^{176}Hf was corrected by measuring the interference-free ^{172}Yb isotope and using the ^{176}Yb/^{172}Yb ratio [*Pearson et al.*, 2008]. The appropriate value of ^{176}Yb/^{172}Yb (0.5865) was determined by successively doping a JMC475 Hf standard (100 ppb solution) with various amounts of Yb and determining the value of ^{176}Yb/^{172}Yb required to yield the value of ^{176}Hf/^{177}Hf in the undoped solution.

Zircons from the Mud Tank carbonatite were periodically analysed as a measure of the accuracy of the results. Most of the data are within 2 standard deviations (SD) of the recommended value (0.282522 ± 0.000042 (2σ)) [*Griffin et al.*, 2007].

Calculation of ε_{Hf} values employed the ^{176}Lu decay constant of *Scherer et al.* [2001] and the CHUR values of *Blichert-Toft and Albarède* [1997]. Weighted mean ^{238}U/^{206}Pb ages for individual samples have been used for calculations of both initial ^{176}Hf/^{177}Hf ratios and ε_{Hf}. Two-stage Depleted-Mantle Model ages have been calculated assuming that the parental magma was produced from an average basalt (^{176}Lu/^{177}Hf = 0.022) [*Lancaster et al.*, 2011] that was originally derived from the Depleted Mantle with initial (^{176}Hf/^{177}Hf)$_i$ = 0.279718 (at 4.56 Ga) and ^{176}Lu/^{177}Hf = 0.0384 [*Griffin et al.*, 2004].

Acknowledgments

The authors thank Ole Balthazar Andersen and the Technical University of Denmark who kindly provided the gravity data. The preparation of this manuscript was supported by the Grant Agency of Czech Republic project P210/12/2205 to K. Schulmann. The support received by K.S. from the Ministry of Education of the Czech Republic (grant LK11202) is also gratefully acknowledged. Chris Stanley (NHM London) kindly improved English style and grammar. The text was also read and improved by a native English speaker Professor Chris Halls from NHM of London who improved our English style whenever he felt our writing style is too much "continental English" without modifying content or message of our text. This is a contribution to IGCP Project 592 sponsored by IUGS and UNESCO. Constructive and stimulating comments of the three reviewers, Rita Economos, Roberto Weinberg, and Min Sun, to the earlier version of this manuscript are gratefully acknowledged. We thank Claudio Faccenna for his editorial work.

References

Amante, C., and B. W. Eakins (2009), ETOPO1 1 Arc-Minute Global Relief Model: Procedures, Data Sources and Analysis, NOAA Technical Memorandum NESDIS NGDC, 19–24.

Andersen, D. J., and D. H. Lindsley (1988), Internally consistent solution models for Fe-Mg-Mn-Ti oxides; Fe-Ti oxides, *Am. Mineral.*, *73*(7–8), 714–726.

Andersen, O. B., and P. Knudsen (2009), DNSC08 mean sea surface and mean dynamic topography models, *J. Geophys. Res.*, *114*, C11001, doi:10.1029/2008JC005179.

Armstrong, R. N., R. Seltmann, D. Crane, and CERCAMS Team (2010), Oyu Tolgoi and porphyries of South Mongolia, *Trans. Inst. Min. Metall. B Appl. Earth Sci.*, *119*(2), 83–84.

Arndt, N., G. Bruzak, and T. Reischmann (2001), The oldest continental and oceanic plateaus: Geochemistry of basalts and komatiites of the Pilbara Craton, Australia, in *Mantle Plumes: Their Identification Through Time*, vol. 352, edited by R. E. Ernst and K. L. Buchan, pp. 359–387, Geol. Soc. Am. Spec. Pap.

Badarch, G., W. Dickson Cunningham, and B. F. Windley (2002), A new terrane subdivision for Mongolia: Implications for the Phanerozoic crustal growth of Central Asia, *J. Asian Earth Sci.*, *21*(1), 87–110.

Barry, T. L., A. D. Saunders, P. D. Kempton, B. F. Windley, M. S. Pringle, D. Dorjnamjaa, and S. Saandar (2003), Petrogenesis of Cenozoic basalts from Mongolia: Evidence for the role of asthenospheric versus metasomatized lithospheric mantle sources, *J. Petrol.*, *44*(1), 55–91.

Belousova, E. A., Y. A. Kostitsyn, W. L. Griffin, G. C. Begg, S. Y. O'Reilly, and N. J. Pearson (2010), The growth of the continental crust: Constraints from zircon Hf-isotope data, *Lithos*, *119*(3–4), 457–466.

Berg, H. C., D. L. Jones, and D. H. Richter (1972), Gravina-Nutzotin Belt: Tectonic significance of an Upper Mesozoic sedimentary and volcanic sequence in southern and southeastern Alaska, *U.S. Geol. Surv. Prof. Pap. 800-D*.

Berg, H. C., D. L. Jones, and P. J. Coney (1978), Map showing pre-Cenozoic tectonostratigraphic terranes of southeastern Alaska and adjacent areas, *U.S. Geol. Surv. Open File Rep.* 78–1085.

Blakely, R. J. (1996), *Potential Theory in Gravity and Magnetic Applications*, 468 pp., Cambridge Univ. Press, Cambridge.

Blichert-Toft, J., and F. Albarède (1997), The Lu-Hf isotope geochemistry of chondrites and the evolution of the mantle-crust system, *Earth Planet. Sci. Lett.*, *148*(1–2), 243–258.

Bonin, B. (2007), A-type granites and related rocks: Evolution of a concept, problems and prospects, *Lithos*, *97*(1–2), 1–29.

Boutelier, D., A. Chemenda, and J. P. Burg (2003), Subduction versus accretion of intra-oceanic volcanic arcs: Insight from thermo-mechanical analogue experiments, *Earth Planet. Sci. Lett.*, *212*(1–2), 31.

Broussolle, A., et al. (2015), P−T−t−D record of crustal-scale horizontal flow and magma assisted doming in the SW Mongolian Altai, *J. Metamorph. Geol.*, *33*, 359–383, doi:10.1111/jmg.12124.

Brown, M. (2007), Crustal melting and melt extraction, ascent and emplacement in orogens: Mechanisms and consequences, *J. Geol. Soc.*, *164*(4), 709–730.

Brown, M. (2013), Granite: From genesis to emplacement, *Geol. Soc. Am. Bull.*, *125*(7–8), 1079–1113.

Burton, G. R. (2010), New structural model to explain geophysical features in northwestern new south wales: Implications for the tectonic framework of the Tasmanides, *Aust. J. Earth Sci.*, *57*(1), 23–49.

Cawood, P. A., A. Kröner, W. J. Collins, T. M. Kusky, W. D. Mooney, and B. F. Windley (2009), Accretionary orogens through Earth history, in *Earth Accretionary Systems in Space and Time*, vol. 318, edited by P. A. Cawood and A. Kröner, pp. 1–36, Geol. Soc. London Spec. Publ.

Chemenda, A. I., J. P. Burg, and M. Mattauer (2000), Evolutionary model of the Himalaya-Tibet system: Geopoem based on new modelling, geological and geophysical data, *Earth Planet. Sci. Lett.*, *174*(3–4), 397–409.

Chen, L., W. Tao, L. Zhao, and T. Zheng (2008), Distinct lateral variation of lithospheric thickness in the Northeastern North China Craton, *Earth Planet. Sci. Lett.*, *267*(1–2), 56–68.

Christensen, N. I., and W. D. Mooney (1995), Seismic velocity structure and composition of the continental crust—A global view, *J. Geophys. Res.*, *100*(B6), 9761–9788, doi:10.1029/95JB00259.

Clemens, J. D. (2003), *S*-type granitic magmas—Petrogenetic issues, models and evidence, *Earth Sci. Rev.*, *61*(1–2), 1–18.

Clemens, J. D. (2012), Granitic magmatism, from source to emplacement: A personal view, *Appl. Earth Sci.*, *121*(3), 107–136.
Coney, P. J., D. L. Jones, and J. W. H. Monger (1980), Cordilleran suspect terranes, *Nature*, *288*(5789), 329–333.
Connolly, J. A. D. (2005), Computation of phase equilibria by linear programming: A tool for geodynamic modeling and its application to subduction zone decarbonation, *Earth Planet. Sci. Lett.*, *236*(1–2), 524–541.
Cunningham, D., S. Davies, and D. McLean (2009), Exhumation of a Cretaceous rift complex within a Late Cenozoic restraining bend, southern Mongolia: Implications for the crustal evolution of the Gobi Altai region, *J. Geol. Soc.*, *166*(2), 321–333.
DeBievre, P., and P. D. P. Taylor (1993), IUPAC recommended isotopic abundances, *Int. J. Mass Spectrom. Ion Phys.*, *149*.
Debon, F., and P. Le Fort (1983), A chemical-mineralogical classification of common plutonic rocks and associations, *Trans. Roy. Soc. Edinburgh Earth Sci.*, *73*, 135–149.
De La Roche, H., J. Leterrier, P. Grandclaude, and M. Marchal (1980), A classification of volcanic and plutonic rocks using R_1R_2-diagram and major element analyses—Its relationships with current nomenclature, *Chem. Geol.*, *29*, 183–210.
Demoux, A., A. Kröner, G. Badarch, P. Jian, D. Tomurhuu, and M. T. D. Wingate (2009), Zircon ages from the Baydrag Block and the Bayankhongor Ophiolite Zone: Time constraints on Late Neoproterozoic to Cambrian subduction- and accretion-related magmatism in central Mongolia, *J. Geol.*, *117*(4), 377–397.
Didenko, A. N., A. A. Mossakovsky, D. M. Pechersky, S. V. Ruzhentsev, S. G. Samygin, and T. N. Kheraskova (1994), Geodynamics of Paleozoic oceans of Central Asia, *Russ. Geol. Geophys.*, *35*(7–8), 59–75 (in Russian).
Dijkstra, A. H., F. M. Brouwer, W. D. Cunningham, C. Buchan, G. Badarch, and P. R. D. Mason (2006), Late Neoproterozoic proto-arc ocean crust in the Dariv Range, Western Mongolia: A supra-subduction zone end-member ophiolite, *J. Geol. Soc.*, *163*(2), 363–373.
Downes, H. (1993), The nature of the lower continental crust of Europe: Petrological and geochemical evidence from xenoliths, *Phys. Earth Planet. Inter.*, *79*(1–2), 195–218.
Dumitru, T. A., and M. S. Hendrix (2001), Fission-track constraints on Jurassic folding and thrusting in southern Mongolia and their relationship to the Beishan thrust belt of northern China, in *Paleozoic and Mesozoic Tectonic Evolution of Central and Eastern Asia: From Continental Assembly to Intracontinental Deformation*, vol. 194, edited by M. S. Hendrix and G. A. Davis, pp. 215–229, Mem. Geol. Soc. Am.
Eby, G. N. (1990), The A-type granitoids: A review of their occurrence and chemical characteristics and speculations on their petrogenesis, *Lithos*, *26*, 115–134.
Economos, R., C. P. Hanžl, K. Hrdličková, D. Buriánek, S. Lkhagva-Ochir, A. Gerdes, and S. R. Paterson (2008), Geochemical and structural constraints on the magmatic history of the Chandman Massif of the eastern Mongolian Altay Range, SW Mongolia, *J. Geosci.*, *53*, 335–352.
Edel, J. B., K. Schulmann, P. Hanžl, and O. Lexa (2014), Palaeomagnetic and structural constraints on 90° anticlockwise rotation in SW Mongolia during the Permo-Triassic: Implications for Altaid oroclinal bending. Preliminary palaeomagnetic results, *J. Asian Earth Sci.*, *94*, 157–171.
Fliedner, M. M., and S. L. Klemperer (2000), Crustal structure transition from oceanic arc to continental arc, eastern Aleutian Islands and Alaska Peninsula, *Earth Planet. Sci. Lett.*, *179*(3–4), 567–579.
Fuhrman, M. L., and D. H. Lindsley, (1988), Ternary-feldspar modeling and thermometry, *Am. Mineralog.*, *73*, 201–215.
Glen, J. M. G., J. Schmidt, and R. Morin (2007), Gravity and magnetic character of south-central Alaska: Constraints on geologic and tectonic interpretations, and implications for mineral exploration, *Geol. Society Am. Spec. Pap.*, *431*, 593–622.
Green, E., T. Holland, and R. Powell (2007), An order-disorder model for omphacitic pyroxenes in the system jadeite-diopside-hedenbergite-acmite, with applications to eclogitic rocks, *Am. Mineral.*, *92*(7), 1181–1189.
Griffin, W. L., E. A. Belousova, S. R. Shee, N. J. Pearson, and S. Y. O'Reilly (2004), Archean crustal evolution in the northern Yilgarn Craton: U-Pb and Hf-isotope evidence from detrital zircons, *Precambrian Res.*, *131*(3–4), 231–282.
Griffin, W. L., N. J. Pearson, E. A. Belousova, and A. Saeed (2007), Reply to "Comment to short-communication 'Comment: Hf-isotope heterogeneity in zircon 91500' by W.L. Griffin, N.J. Pearson, E.A. Belousova and A. Saeed (Chemical Geology 233 (2006) 358–363)" by F. Corfu, *Chem. Geol.*, *244*, 354–356.
Guy, A., K. Schulmann, N. Clauer, P. Hasalová, R. Seltmann, R. Armstrong, O. Lexa, and A. Benedicto (2014a), Late Paleozoic–Mesozoic tectonic evolution of the Trans-Altai and South Gobi zones in southern Mongolia based on structural and geochronological data, *Gondwana Res.*, *25*, 309–337.
Guy, A., K. Schulmann, M. Munschy, J.-M. Miehe, J.-B. Edel, O. Lexa, and D. Fairhead (2014b), Geophysical constraints for terrane boundaries in southern Mongolia, *J. Geophys. Res. Solid Earth*, *119*, 7966–7991, doi:10.1002/2014JB011026.
Hacker, B. R., P. B. Kelemen, and M. D. Behn (2011), Differentiation of the continental crust by relamination, *Earth Planet. Sci. Lett.*, *307*(3–4), 501–516.
Hanžl, P., D. Buriánek, A. Gerdes, K. Hrdličková, V. Janoušek, K. Schulmann (2014), The Cambrian magmatic activity in the Zamtyn Nuruu range, Mongolian Altai, in Zelazniewicz, A., Jastrzebski, M., Twyrdy, M: The 2014 CETEG Conference "Ladek", Proceedings and Excursion Guide, Geologia Sudetica, 42., p. 25.
Harris, N. B. W., and S. Inger (1992), Trace element modelling of pelite-derived granites, *Contrib. Mineral. Petrol.*, *110*(1), 46–56.
Hawkesworth, C. J., B. Dhuime, A. B. Pietranik, P. A. Cawood, A. I. S. Kemp, and C. D. Storey (2010), The generation and evolution of the continental crust, *J. Geol. Soc.*, *167*(2), 229–248.
Helo, C., E. Hegner, A. Kröner, G. Badarch, O. Tomurtogoo, B. F. Windley, and P. Dulski (2006), Geochemical signature of Paleozoic accretionary complexes of the Central Asian Orogenic Belt in South Mongolia: Constraints on arc environments and crustal growth, *Chem. Geol.*, *227*(3–4), 236–257.
Holbrook, W. S., D. Lizarralde, S. McGeary, N. Bangs, and J. Diebold (1999), Structure and composition of the Aleutian island arc and implications for continental crustal growth, *Geology*, *27*(1), 31–34.
Holland, T. J. B., and R. Powell (1998), An internally consistent thermodynamic data set for phases of petrological interest, *J. Metamorph. Geol.*, *16*(3), 309–343.
Ionov, D. (2002), Mantle structure and rifting processes in the Baikal-Mongolia region: Geophysical data and evidence from xenoliths in volcanic rocks, *Tectonophysics*, *351*(1–2), 41–60.
Jahn, B. M. (2004), The Central Asian Orogenic Belt and growth of the continental crust in the Phanerozoic, in *Aspects of the Tectonic Evolution of China*, vol. 226, edited by J. Malpas et al., pp. 73–100, Geol. Soc. London Spec. Publ.
Janoušek, V., C. M. Farrow, and V. Erban (2006), Interpretation of whole-rock geochemical data in igneous geochemistry: Introducing Geochemical Data Toolkit (GCDkit), *J. Petrol.*, *47*(6), 1255–1259.
Janoušek, V., J. Konopásek, S. Ulrich, V. Erban, L. Tajčmanová, and P. Jeřábek (2010), Geochemical character and petrogenesis of Pan-African Amspoort suite of the Boundary Igneous Complex in the Kaoko Belt (NW Namibia), *Gondwana Res.*, *18*(4), 688–707.
Janoušek, V., Y. Jiang, K. Schulmann, D. Buriánek, P. Hanžl, O. Lexa, T. Ganchuluun, and B. Altanbaatar (2014), The age, nature and likely genesis of the Cambrian Khantaishir arc, Lake Zone, Mongolia, Geophys. Res., 16, EGU2014-6108.

Jian, P., A. Kröner, B.-m. Jahn, B. F. Windley, Y. Shi, W. Zhang, F. Zhang, L. Miao, D. Tomurhuu, and D. Liu (2014), Zircon dating of Neoproterozoic and Cambrian ophiolites in West Mongolia and implications for the timing of orogenic processes in the central part of the Central Asian Orogenic Belt, *Earth Sci. Rev.*, *133*, 62–93.

Johannes, W., and F. Holtz (1996), *Petrogenesis and Experimental Petrology of Granitic Rocks*, pp. 335, Springer, Berlin.

Johnson, C. L., J. A. Amory, D. Zinniker, M. A. Lamb, S. A. Graham, M. Affolter, and G. Badarch (2008), Sedimentary response to arc-continent collision, Permian, southern Mongolia, *Geol. Soc. Am. Spec. Pap.*, *436*, 363–390.

Jones, D. L., D. G. Howell, P. J. Coney, and J. W. H. Monger (1983), Recognition, character, and analysis of tectonostratigraphic terranes in western North America, Accretion tectonics in the circum-Pacific regions, Proc. seminar, 1981, Tomakomai, 21–35.

Jung, S., P. Masberg, D. Mihm, and S. Hoernes (2009), Partial melting of diverse crustal sources—Constraints from Sr-Nd-O isotope compositions of quartz diorite-granodiorite-leucogranite associations (Kaoko Belt, Namibia), *Lithos*, *111*(3–4), 236–251.

Kemp, A. I. S., and C. J. Hawkesworth (2003), Granitic perspectives on the generation and secular evolution of the continental crust, in *Treatise on Geochemistry*, edited by R. L. Rudnick, pp. 349–410, Elsevier, Oxford.

Kemp, A. I. S., and C. J. Hawkesworth (2014), Growth and differentiation of the continental crust from isotope studies of accessory minerals, in *Treatise on Geochemistry (Second Edition)*, edited by H. D. Holland and K. K. Turekian, pp. 379–421, Elsevier, Oxford.

Khain, E. V., E. V. Bibikova, E. B. Salnikova, A. Kröner, A. S. Gibsher, A. N. Didenko, K. E. Degtyarev, and A. A. Fedotova (2003), The Palaeo-Asian ocean in the Neoproterozoic and Early Palaeozoic: New geochronologic data and palaeotectonic reconstructions, *Precambrian Res.*, *122*(1–4), 329–358.

Kopylova, M. G., S. Y. O'Reilly, and Y. S. Genshaft (1995), Thermal state of the lithosphere beneath Central Mongolia: Evidence from deep-seated xenoliths from the Shavaryn-Saram volcanic centre in the Tariat depression, Hangai, Mongolia, *Lithos*, *36*(3–4), 243–255.

Kovalenko, V. I., V. V. Yarmolyuk, V. P. Kovach, A. B. Kotov, I. K. Kozakov, E. B. Sal'Nikova, and A. M. Larin (2004), Isotope provinces, mechanisms of generation and sources of the continental crust in the Central Asian mobile belt: Geological and isotopic evidence, *J. Asian Earth Sci.*, *23*(5), 605–627.

Kozakov, I. K., A. B. Kotov, V. P. Kovach, and E. B. Salnikova (1997), Crustal growth in the geologic evolution of the Baidrag block, Central Mongolia: Evidence from Sm-Nd isotopic systematics, *Petrology*, *5*(3), 227–235.

Kozakov, I. K., E. V. Bibikova, P. Y. Azimov, and T. I. Kirnozova (2002a), Hercynian granulites of Mongolian and Gobian Altai: Geodynamic setting and formation conditions, *Dokl. Earth Sci.*, *386*(7), 781–785.

Kozakov, I. K., E. B. Sal'nikova, E. V. Khain, V. P. Kovach, N. G. Berezhnaya, S. Z. Yakovleva, and Y. V. Plotkina (2002b), Early Caledonian crystalline rocks of the Lake Zone in Mongolia: Formation history and tectonic settings as deduced from U-Pb and Sm-Nd datings, *Geotectonics*, *36*, 156–166.

Kröner, A., J. Lehmann, K. Schulmann, A. Demoux, O. Lexa, D. Tomurhuu, P. Štípská, D. Otgonbator, D. Y. Liu, and M. T. D. Wingate (2010), Lithostratigraphic and geochronological constraints on the evolution of the Central Asian Orogenic Belt in SW Mongolia: Early Paleozoic rifting followed by Late Paleozoic accretion, *Am. J. Sci.*, *310*, 523–574.

Kröner, A., et al. (2014), Reassessment of continental growth during the accretionary history of the Central Asian Orogenic Belt, *Gondwana Res.*, *25*, 103–125.

Lamb, M. A., and G. Badarch (2001), Paleozoic sedimentary basins and volcanic arc systems of southern Mongolia: New geochemical and petrographic constraints, in *Paleozoic and Mesozoic Tectonic Evolution of Central and Eastern Asia: From Continental Assembly to Intracontinental Deformation*, edited by M. S. Hendrix and G. A. Davis, pp. 117–149, Memoir of the Geological Society of America.

Lancaster, P. J., C. D. Storey, C. J. Hawkesworth, and B. Dhuime (2011), Understanding the roles of crustal growth and preservation in the detrital zircon record, *Earth Planet. Sci. Lett.*, *305*(3–4), 405–412.

Lehmann, J., K. Schulmann, O. Lexa, M. Corsini, A. Kröner, P. Štípská, D. Tomurhuu, and D. Otgonbator (2010), Structural constraints on the evolution of the Central Asian Orogenic Belt in SW Mongolia, *Am. J. Sci.*, *310*, 575–628.

Leonov, M. G. (2012), Within-plate zones of concentrated deformation: Tectonic structure and evolution, *Geotectonics*, *46*(6), 389–411.

Ludwig, K. R. (1999), User's Manual for Isoplot/Ex, Version 2.10: A geochronological toolkit for Microsoft Excel, Berkeley Geochronology Center Special Publication 1a, Berkeley, Calif.

Ludwig, K. R. (2000), SQUID 1.00: A User's Manual, Berkeley Geochronology Center Special Publication 2, Berkeley, Calif.

Miller, H. G., and V. Singh (1994), Potential field tilt—A new concept for location of potential field sources, *J. Appl. Geophys.*, *32*(2–3), 213–217.

Monger, J. W. H., R. A. Price, and D. J. Tempelmankluit (1982), Tectonic accretion and the origin of the 2 major metamorphic and plutonic belts in the Canadian Cordillera, *Geology*, *10*(2), 70–75.

Moore, J. C., et al. (1991), EDGE deep seismic reflection transect of the eastern Aleutian arc-trench layered lower crust reveals underplating and continental growth, *Geology*, *19*(5), 420–424.

Mordvinova, V. V., and A. A. Artemyev (2010), The three-dimensional shear velocity structure of lithosphere in the southern Baikal rift system and its surroundings, *Russ. Geol. Geophys.*, *51*(6), 694–707.

Mordvinova, V. V., A. Deschamps, T. Dugarmaa, J. Deverchére, M. Ulziibat, V. A. Sankov, A. A. Artemyev, and J. Perrot (2007), Velocity structure of the lithosphere on the 2003 Mongolian-Baikal transect from SV waves, Izvestiya, *Phys. Solid Earth*, *43*(2), 119–129.

Patiño Douce, A. E. (1997), Generation of metaluminous A-type granites by low-pressure melting of calc-alkaline granitoids, *Geology*, *25*(8), 743–746.

Patiño Douce, A. E., and T. C. McCarthy (1998), Melting of crustal rocks during continental collision and subduction, in *When Continents Collide: Geodynamics and Geochemistry of Ultrahigh-Pressure Rocks*, edited by B. Hacker and J. Liou, pp. 27–55, Springer, Netherlands.

Pearce, J. A., N. W. Harris, and A. G. Tindle (1984), Trace element discrimination diagrams for the tectonic interpretation of granitic rocks, *J. Petrol.*, *25*, 956–983.

Pearson, N. J., W. L. Griffin, and S. Y. O'Reilly (2008), Mass fractionation correction in laser ablation multiple-collector ICP-MS: Implications for overlap corrections and precise and accurate in situ isotope ratio measurement, in *Laser-Ablation-ICP-MS in the Earth Sciences: Current Practices and Outstanding Issues*, edited by P. J. Sylvester, pp. 93–116, Mineralog. Assoc. of Canada Short Course Ser., Vancouver, B. C.

Peccerillo, A., and S. R. Taylor (1976), Geochemistry of Eocene calc-alkaline volcanic rocks from the Kastamonu area, Northern Turkey, *Contrib. Mineral. Petrol.*, *58*, 63–81.

Petit, C., J. Déverchère, E. Calais, V. San'kov, and D. Fairhead (2002), Deep structure and mechanical behavior of the lithosphere in the Hangai-Hövsgöl region, Mongolia: New constraints from gravity modeling, *Earth Planet. Sci. Lett.*, *197*(3–4), 133–149.

Petit, C., C. Tiberi, A. Deschamps, and J. Déverchère (2008), Teleseismic traveltimes, topography and the lithospheric structure across central Mongolia, *Geophys. Res. Lett.*, *35*, L11301, doi:10.1029/2008GL033993.

Powell, R., and T. Holland (1999), Relating formulations of the thermodynamics of mineral solid solutions: Activity modeling of pyroxenes, amphiboles, and micas, *Am. Mineral.*, *84*(1–2), 1–14.

Roberts, M. P., and J. D. Clemens (1993), Origin of high-potassium, calc-alkaline, I-type granitoids, *Geology*, *21*, 825–828.

Rojas-Agramonte, Y., A. Kröner, A. Demoux, X. Xia, W. Wang, T. Donskaya, D. Liu, and M. Sun (2011), Detrital and xenocrystic zircon ages from Neoproterozoic to Palaeozoic arc terranes of Mongolia: Significance for the origin of crustal fragments in the Central Asian Orogenic Belt, *Gondwana Res.*, *19*(3), 751–763.
Rudnick, R. L. (1992), Xenoliths—Samples of the lower continental crust, in *Continental Lower Crust*, edited by D. Fountain, M. R. Arculus, and R. W. Kay, pp. 269–316, Elsevier, Amsterdam.
Rudnick, R. L., and D. M. Fountain (1995), Nature and composition of the continental crust—A lower crustal perspective, *Rev. Geophys.*, *33*, 267–309, doi:10.1029/95RG01302.
Ruzhentsev, S. V. (2001), The Variscan belt of south Mongolia and Dzungaria, in *Tectonics, Magmatism, and Metallogeny of Mongolia*, edited by A. B. Dergunov, pp. 61–94, Routledge, London.
Ruzhentsev, S. V., G. Badarch, and T. A. Voznesenskaya (1985), Tectonics of the Trans-Altai zone of Mongolia (Gurvansaykhan and Dzolen ranges), *Geotectonics*, *19*, 276–284.
Ruzhentsev, S. V., I. Pospelov, and G. Badarch (1992), The Inner-Mongolia ophiolitic sutures, *Doklady Akad. Nauk SSSR*, *322*(5), 953–958.
Safonova, I., R. Seltmann, A. Kröner, D. Gladkochub, K. Schulmann, W. Xiao, J. Kim, T. Komiya, and M. Sun (2011), A new concept of continental construction in the Central Asian Orogenic Belt (compared to actualistic examples from the Western Pacific), *Episodes*, *34*(3), 186–196.
Sato, T., T. No, S. Kodaira, N. Takahashi, and Y. Kaneda (2014), Seismic constraints of the formation process on the back-arc basin in the southeastern Japan Sea, *J. Geophys. Res. Solid Earth*, *119*, 1563–1579, doi:10.1002/2013JB010643.
Saunders, A. D., J. Tarney, A. C. Kerr, and R. W. Kent (1996), The formation and fate of large oceanic igneous provinces, *Lithos*, *37*(2–3), 81–95.
Scherer, E., C. Monker, and K. Mezger (2001), Calibration of the lutetium-hafnium clock, *Science*, *293*(5530), 683–687.
Schulmann, K., and S. Paterson (2011), Geodynamics: Asian continental growth, *Nat. Geosci.*, *4*(12), 827–829.
Schulmann, K., O. Lexa, V. Janoušek, J. M. Lardeaux, and J. B. Edel (2014), Anatomy of a diffuse cryptic suture zone: An example from the Bohemian Massif, European Variscides, *Geology*, *42*(4), 275–278.
Seltmann, R., D. Konopelko, G. Biske, F. Divaev, and S. Sergeev (2011), Hercynian post-collisional magmatism in the context of Paleozoic magmatic evolution of the Tien Shan orogenic belt, *J. Asian Earth Sci.*, *42*(5), 821–838.
Şengör, A. M. C., and B. A. Natal'in (1996), Palaeotectonics of Asia: Fragments of a synthesis, in *The Tectonic Evolution of Asia*, edited by C. U. P. Rubey Colloquium, pp. 486–640, Cambridge Univ. Press, Cambridge.
Şengör, A. M. C., B. A. Natal'in, and V. S. Burtman (1993), Evolution of the Altaid tectonic collage and Paleozoic crustal growth in Eurasia, *Nature*, *364*, 299–307.
Skjerlie, K. P., and A. D. Johnston (1992), Vapor-absent melting at 10 kbar of a biotite- and amphibole-bearing tonalitic gneiss: Implications for the generation of A-type granites, *Geology*, *20*, 263–266.
Spakman, W., and R. Hall (2010), Surface deformation and slab-mantle interaction during Banda arc subduction rollback, *Nat. Geosci.*, *3*(8), 562–566.
Stacey, J. S., and J. D. Kramers (1975), Approximation of terrestrial lead isotope evolution by a two-stage model, *Earth Planet. Sci. Lett.*, *26*(2), 207–221.
Štípská, P., K. Schulmann, J. Lehmann, M. Corsini, O. Lexa, and D. Tomurhuu (2010), Early Cambrian eclogites in SW Mongolia: Evidence that the Palaeo-Asian Ocean suture extends further east than expected, *J. Metamorph. Geol.*, *28*(9), 915–933.
Stosch, H. G., D. A. Ionov, I. S. Puchtel, S. J. G. Galer, and A. Sharpouri (1995), Lower crustal xenoliths from Mongolia and their bearing on the nature of the deep crust beneath central Asia, *Lithos*, *36*(3–4), 227–242.
Suyetenko, O. D., Y. V. Golovchenko, G. M. Dobrov, and A. B. Tsukernik (1988), Paleozoic structures in the Transaltay Gobi, *Izv. Akad. Nauk SSSR Ser. Geol.*, *4*, 64–76.
Sylvester, P. J. (1998), Post-collisional strongly peraluminous granites, *Lithos*, *45*, 29–44.
Taylor, S. R., and S. M. McLennan (1995), The geochemical evolution of the continental crust, *Rev. Geophys.*, *33*, 241–265, doi:10.1029/95RG00262.
Telford, W. M., L. P. Geldart, and R. E. Sheriff (1990), *Applied Geophysics*, 2nd ed., Cambridge Univ. Press, Cambridge.
Teng, J., Z. Zhang, X. Zhang, C. Wang, R. Gao, B. Yang, Y. Qiao, and Y. Deng (2013), Investigation of the Moho discontinuity beneath the Chinese mainland using deep seismic sounding profiles, *Tectonophysics*, *609*, 202–216.
Veenstra, E., D. H. Christensen, G. A. Abers, and A. Ferris (2006), Crustal thickness variation in south-central Alaska, *Geology*, *34*(9), 781–784.
Villaseca, C., L. Barbero, and V. Herreros (1998), A re-examination of the typology of peraluminous granite types in intracontinental orogenic belts, *Transactions of the Royal Society of Edinburgh: Earth Sciences*, *89*(2), 113–119.
Wang, Y., W. D. Mooney, X. Yuan, and N. Okaya (2013), Crustal structure of the northeastern Tibetan Plateau from the southern Tarim Basin to the Sichuan Basin, China, *Tectonophysics*, *584*, 191–208.
Weinberg, R. F., and P. Hasalová (2015), Water-fluxed melting of the continental crust: A review, *Lithos*, *212–215*, 158–188.
Wellman, P. (1988), Development of the Australian Proterozoic crust as inferred from gravity and magnetic anomalies, *Precambrian Res.*, *40–1*, 89–100.
Whalen, J. B., K. L. Currie, and B. W. Chappell (1987), A-type granites: Geochemical characteristics, discrimination and petrogenesis, *Contrib. Mineral. Petrol.*, *95*, 407–419.
White, R. W., R. Powell, and T. J. B. Holland (2007), Progress relating to calculation of partial melting equilibria for metapelites, *J. Metamorph. Geol.*, *25*(5), 511–527.
Wiedenbeck, M., P. Allé, F. Corfu, W. L. Griffin, M. Meier, F. Oberli, A. V. Quadt, J. C. Roddick, and W. Spiegel (1995), Three natural zircon standards for U-Th-Pb, Lu-Hf, trace element and REE analyses, *Geostand. Newsl.*, *19*(1), 1–23.
Williams, I. S. (1998), U-Th-Pb geochronology by ion microprobe, in *Applications of Microanalytical Techniques to Understanding Mineralizing Processes*, Rev. Econ. Geol., vol. 7, edited by M. A. McKibben, W. C. Shanks III, and W. I. Ridley, pp. 1–35.
Windley, B. F., D. Alexeiev, W. Xiao, A. Kröner, and G. Badarch (2007), Tectonic models for accretion of the Central Asian Orogenic Belt, *J. Geol. Soc.*, *164*(1), 31–47.
Xiao, W., B. Huang, C. Han, S. Sun, and J. Li (2010), A review of the western part of the Altaids: A key to understanding the architecture of accretionary orogens, *Gondwana Res.*, *18*(2–3), 253–273.
Yarmolyuk, V. V., V. P. Kovach, V. I. Kovalenko, L. B. Terent'eva, I. K. Kozakov, A. B. Kotov, and G. Eenjin (2007), Isotopic composition of the Hercynian crust of southern Mongolia: Substantiation of the Hercynian juvenile crust-forming event, *Dokl. Earth Sci.*, *417*(1), 1178–1182.
Yarmolyuk, V. V., V. I. Kovalenko, A. M. Kozlovsky, V. P. Kovach, E. B. Sal'Nikova, D. V. Kovalenko, A. B. Kotov, E. A. Kudryashova, V. I. Lebedev, and G. Eenzhin (2008), Crust-building processes in the Hercynides of the Central Asian Foldbelt, *Petrology*, *16*(7), 679–709.
Yarmolyuk, V. V., V. P. Kovach, I. K. Kozakov, A. M. Kozlovsky, A. B. Kotov, and E. Y. Rytsk (2012), Mechanisms of continental crust formation in the Central Asian Foldbelt, *Geotectonics*, *46*(4), 251–272.
Yarmolyuk, V. V., M. I. Kuzmin, and A. M. Kozlovsky (2013), Late Paleozoic–Early Mesozoic within-plate magmatism in North Asia: Traps, rifts, giant batholiths, and the geodynamics of their origin, *Petrology*, *21*(2), 101–126.

Zhang, S., et al. (2014), Crustal structures revealed from a deep seismic reflection profile across the Solonker suture zone of the Central Asian Orogenic Belt, northern China: An integrated interpretation, *Tectonophysics*, *612–613*, 26–39.
Zonenshain, L. P. (1973), The evolution of Central Asiatic geosynclines through sea-floor spreading, *Tectonophysics*, *19*(3), 213–232.
Zonenshain, L. P., and M. I. Kuzmin (1978), Khantaishir ophiolite complex in western Mongolia and ophiolite problem, *Geotectonics*, *1*, 19–42.
Zonenshain, L. P., O. D. Suyetenko, L. Jamyandamba, and G. Eengin (1975), Structure and the axial part of South Mongolian eugeosyncline in the Dzolen Range, *Geotectonics*, *4*, 28–44.
Zorin, Y. A., et al. (1993), The South Siberia–Central Mongolia transect, *Tectonophysics*, *225*(4), 361.